# ImmunoPEGliposomes for the targeted delivery of novel lipophilic drugs to red blood cells in a falciparum malaria murine model

Ernest Moles[a,b,c,*], Silvia Galiano[d,e], Ana Gomes[f], Miguel Quiliano[d,e], Cátia Teixeira[f], Ignacio Aldana[d,e], Paula Gomes[f], Xavier Fernàndez-Busquets[a,b,c,*]

[a] Nanomalaria Group, Institute for Bioengineering of Catalonia (IBEC), The Barcelona Institute of Science and Technology, Baldiri Reixac 10-12, ES-08028 Barcelona, Spain
[b] Barcelona Institute for Global Health (ISGlobal), Barcelona Center for International Health Research (CRESIB, Hospital Clínic-Universitat de Barcelona), Rosselló 149-153, ES-08036 Barcelona, Spain
[c] Nanoscience and Nanotechnology Institute (IN2UB), University of Barcelona, Martí i Franquès 1, ES-08028 Barcelona, Spain
[d] Universidad de Navarra, Instituto de Salud Tropical (ISTUN), Campus Universitario, ES-31008 Pamplona, Spain
[e] Universidad de Navarra, Facultad de Farmacia y Nutrición, Departamento de Química Orgánica y Farmacéutica, Campus Universitario, ES-31008 Pamplona, Spain
[f] LAQV-REQUIMTE, Departamento de Química e Bioquímica, Faculdade de Ciências, Universidade do Porto, Rua do Campo Alegre 685, P-4169-007 Porto, Portugal

* Corresponding authors at: Nanomalaria Group, Barcelona Institute for Global Health (ISGlobal), Rosselló 149-153, ES-08036 Barcelona, Spain.
*E-mail addresses*: ernest.moles@isglobal.org; xfernandez_busquets@ub.edu

**ABSTRACT**

Most drugs currently entering the clinical pipeline for severe malaria therapeutics are of lipophilic nature, with a relatively poor solubility in plasma and large biodistribution volumes. Low amounts of these compounds do consequently accumulate in circulating *Plasmodium*-infected red blood cells, exhibiting limited antiparasitic activity. These drawbacks can in principle be satisfactorily dealt with by stably encapsulating drugs in targeted nanocarriers. Here this approach has been adapted for its use in immunocompetent mice infected by the *Plasmodium yoelii* 17XL lethal strain, selected as a model for human blood infections by *Plasmodium falciparum*. Using immunoliposomes targeted against a surface protein characteristic of the murine erythroid lineage, the protocol has been applied to two novel antimalarial lipophilic drug candidates, an aminoquinoline and an aminoalcohol. Large encapsulation yields of >90% were obtained using a citrate-buffered pH gradient method and the resulting immunoliposomes reached *in vivo* erythrocyte targeting and retention efficacies of >80%. In *P. yoelii*-infected mice, the immunoliposomized aminoquinoline succeeded in decreasing blood parasitemia from severe to uncomplicated malaria parasite densities (i.e. from ≥25% to ca. 5%), whereas the same amount of drug encapsulated in non-targeted liposomes had no significant effect on parasite growth. Pharmacokinetic analysis indicated that this good performance was obtained with a rapid clearance of immunoliposomes from the circulation (blood half-life of ca. 2 h), indicating a potential for improvement of the proposed model.

**Keywords:** immunoliposomes; malaria; nanomedicine; *Plasmodium falciparum*; *Plasmodium yoelii* 17XL; targeted drug delivery.

## 1. Introduction

Malaria is one of the most devastating parasitic diseases affecting humans and a prominent global health concern, causing nearly half million deaths worldwide every year [1]. Most severe clinical manifestations, in which patients are frequently unable to take oral solid medications and high parasite densities are consistently found [2], are derived from the *Plasmodium falciparum* intraerythrocytic cycle [3,4]. For this reason, the blood stages of the pathogen have been widely considered for the development of several red blood cell (RBC) and/or parasitized RBC (pRBC)-targeted antimalarial approaches based on the use of liposomal and polymeric drug nanocarriers [5-11]. These strategies rely mostly on the cell-specific delivery of nanoparticle payloads in order to improve the shortcomings commonly associated with the pharmacokinetics and pharmacodynamics of current antimalarial compounds. These are mainly high biodistribution volumes and low effective local drug concentrations particularly in the case of easily metabolized and poorly water-soluble compounds [12-15], which incur the risk of generating resistant parasites [2,16,17]. As a consequence, the administration of high drug doses to the patient is required for a proper antimalarial effect, which results in an increased likelihood of causing toxic side effects.

RBCs offer opportunities in drug delivery systems, either functioning as long-circulating carriers for biologically active compounds [18] and/or providing numerous anchoring points for the attachment of nanoparticles [11,19,20]. Mature erythrocytes exhibit in this regard several attractive and exploitable features that include (i) minimal or absent MHC class I antigen presentation which masks this cell type from the immune system surveillance [21], (ii) absence of intracellular organelles along with minimal metabolic activity restricted to glycolysis maintenance through the Embden-Meyerhof pathway, generation of reductive potential for protection against oxidative stress and oxygen/carbon dioxide transport [22], (iii) a sialic acid-rich glycocalyx which together with the preferential localization of negatively charged lipids in the inner plasma membrane of the cell [23] provides a good retention of positively ionized, weakly basic compounds, and (iv) a large intracellular volume of ca. 90 fL [24,25]. Nevertheless, the use of RBCs as carriers requires tedious processes like a prior *ex vivo* cell manipulation step (e.g. intracellular drug loading or the covalent attachment of functional molecules to the RBC surface) for later reinfusion into compatible receptors [18].

Erythroid-specific markers are abundant on the RBC surface and are widely conserved among humans [26-31] when compared to the highly polymorphic parasite proteins exported to the pRBC membrane [32-34], and their presence is not affected by

*P. falciparum* infection [11]. These features allow for the design of novel combinatorial strategies relying on both antimalarial therapy and its prophylaxis, although such approach has been barely explored against bloodborne infectious disease. Preliminary assays were conducted using passively-loaded chloroquine (CQ) into RBC-targeted immunoliposomes (iLPs), which resulted in significant *Plasmodium berghei* growth inhibition when compared to administration of the free compound [9]. However, only 20% of the injected iLPs bound circulating RBCs, possibly due to poor antibody recognition of target cells. Other common obstacles include limitations in the intracellular loading of drugs due to the lack of endocytic activity taking place at the surface of RBCs and pRBCs [35], and little evaluation of the LP encapsulation capacity of drugs exhibiting distinct physicochemical properties (e.g. charge and hydrophilic vs. lipophilic nature). A previously proposed iLP nanocarrier targeted against human glycophorin A (GPA), an erythroid lineage-specific protein, has displayed the best [RBC+pRBC] *in vitro* targeting efficacies and retention yields obtained so far (~100% after only 15 min exposure time to cells) and provided a significant improvement in CQ antimalarial activity *in vivo*, clearing *P. falciparum* parasitemia to below detectable levels (<0.01%) in a humanized mouse malaria model after a 4-day dosage regimen of 0.5 mg/kg [11]. Intracellular delivery of the encapsulated cargo was suggested to occur mainly by a sustained release process taking place at the targeted cell surface. The use of an active encapsulation strategy relying on the generation of a pH gradient [36-38] offered a highly efficient encapsulation and stable retention of the weakly basic antimalarial compounds CQ and primaquine.

Nevertheless, several weaknesses must be addressed before advancing this immunoliposomal approach into the clinical pipeline. The aforesaid outstanding performance of anti-GPA iLPs was evaluated in immunosuppressed mice engrafted with human erythrocytes in circulation, where the animals presented impaired innate and adaptive immune responses along with low blood parasite densities not exceeding 1-3% parasitemia (i.e. uncomplicated malaria clinical feature) [11,39-41]. Moreover, iLP binding to GPA resulted in considerable cell-agglutinating events when exceeding 10 µM lipid amounts *in vitro* [11], which limited the administration of large drug payloads *in vivo*. Exploring RBC-targeted therapeutics in a fully immunocompetent mouse model for falciparum malaria (i.e. mice infected with *P. yoelii* 17XL as murine-specific lethal strain effectively reproducing *P. falciparum* blood infection in humans [42]) is therefore a necessary step in order to properly validate antiparasitic efficacy in a severe malaria setting, and where the immune response of the host towards the delivered nanoparticles is not suppressed. Furthermore, the availability of a liposomal structure suitable for the encapsulation of lipophilic drugs is crucial in order to enlarge the

number of antimalarial agents capable of being intravenously delivered. This route of administration is required when handling severe malaria clinical processes, and is mainly limited at present to hydrophilic/amphiphilic drug formulations [2]. Finally, in accordance with WHO guidelines updates, CQ is no longer considered as gold standard for malaria therapy due to the massive worldwide appearance of *Plasmodium* resistant strains [2,17]. These considerations have prompted us to research novel drug derivatives capable of overcoming parasite resistance mechanisms and to explore a targeted method for rapid delivery to the circulating parasitized cells before the carrier is cleared from blood.

## 2. Materials and methods

### *2.1. Materials*

Except where otherwise indicated, reagents were purchased from Merck & Co., Inc. (Kenilworth, NJ, USA), and reactions were performed at room temperature (22 to 24 °C). The lipids (all ≥99% purity according to thin layer chromatography analysis) 1,2-distearoyl-*sn*-glycero-3-phosphocholine (DSPC), 1,2-dioleoyl-*sn*-glycero-3-phosphocholine (DOPC), 1,2-distearoyl-*sn*-glycero-3-phosphoethanolamine-N-[maleimide(polyethylene glycol)-2000] (DSPE-PEG2000-Mal), and 1,2-dioleoyl-*sn*-glycero-3-phosphoethanolamine-N-[lissamine rhodamine B sulfonyl] (DOPE-Rho) were purchased from Avanti Polar Lipids, Inc. (Alabaster, AL, USA). Mouse monoclonal IgG2b anti-human GPA (SM3141P) and rat monoclonal IgG2b anti-mouse TER-119 (AM31858PU-N) antibodies were purchased from Acris Antibodies GmbH (OriGene Company, Herford, Germany).

Lipophilic aminoquinolines 7c and 7d, formerly found to display potent *in vitro* activity against intraerythrocytic chloroquine-sensitive and resistant *P. falciparum* parasites [13], were synthesized as heterocyclic-cinnamic conjugates maintaining a chloroquine backbone structure and characterized following previously reported methods [13,43]. The aminoalcohols BCN-01 and BCN-02, showing high *in vitro* and *in vivo* antiplasmodial efficacy against multidrug-resistant strains of *P. falciparum* and a murine model of *P. berghei*, were synthesized and chemically characterized as formerly described [12]. 10 mM stocks for these weakly basic compounds were prepared in methanol; because of their rapid aggregative properties in water-based solutions, non-encapsulated 7c/d and BCN-01/02 for *in vivo* assays were formulated in 10% v/v chloroform/aqueous emulsion. Unless otherwise indicated, ionization relevant

pKa values at physiological pH and drug partition coefficients (log *P*) were calculated *in silico* using the Chemicalize software developed by ChemAxon Ltd [44].

*2.2. Preparation of liposomes and encapsulation of drugs*

Liposomes (LPs) were prepared by the lipid film rehydration method [45]; the formulation DOPC:cholesterol:DSPE-PEG2000-Mal:DOPE-Rho, 84.5:10:5:0.5 was used for the encapsulation of lipophilic compounds, whereas for hydrophilic drug encapsulation DSPC (i.e. saturated-type phosphatidylcholine, PC) substituted for DOPC (i.e. unsaturated-type PC) to reduce membrane fluidity and permeability. Briefly, stock lipids in chloroform were mixed and dissolved in chloroform:methanol (2:1 v/v) in a round-bottom flask and organic solvents were subsequently removed by rotary evaporation under reduced pressure at 37 °C. Except where otherwise noted, the dried lipid film was hydrated in phosphate-buffered saline (PBS) supplemented with 10 mM ethylenediaminetetraacetic acid (EDTA) isotonic to Roswell Park Memorial Institute (RPMI) complete medium used for *P. falciparum* culture and containing Albumax II (RPMI-A, Invitrogen). Unilamellar vesicles were then obtained by 4 cycles of constant vortexing along with bath sonication (3 min each), followed by extrusion through 400 nm polycarbonate membranes in an extruder device (Avanti Polar Lipids, Inc.). Throughout the lipid film hydration and downsizing processes, samples were maintained above the lipids' transition temperature. Sterility of LP samples was maintained by rinsing all material in 70% ethanol and working in a laminar flow hood. LP ζ-potential determination and dynamic light scattering size measurements were done after 1:30 sample dilution in either deionized water (Milli-Q® system, Millipore) or PBS, using a Zetasizer NanoZS90 (Malvern Ltd, Malvern, UK). Unencapsulated material was removed by buffer exchange in 7-kDa Zeba™ spin desalting columns (Thermo Fisher Scientific, Inc.) using isotonic PBS. For drug encapsulation, lipophilic compounds already solubilized in organic solvents were directly added into the initial lipid mixture (DOPC-based) at a 1:40 or 1:10 drug:lipid ratio for *in vitro* and *in vivo* applications, respectively, whereas hydrophilic drugs were incorporated in the lipid hydrating buffer upon LP formation (DSPC-based). Active encapsulation of drugs through citrate-based pH gradient formation (citric acid, pH 4.0/PBS, pH 7.4 as inner/outer aqueous phases of LP suspensions) was conducted according to previously established protocols [11]. When including pyranine in the lipid film hydration solution for tracking purposes, PBS-EDTA, pH 6.5, was used as solvent according to [5]. Encapsulation efficiency is expressed as the percentage of encapsulated drug relative to the total amount initially added to the liposomal sample. Data are represented as the

mean ± standard deviation of at least three independent measurements. Following previously established protocols [5,11], drug release from LP samples was determined at specific time points after removal of non-encapsulated material by ultracentrifugation (150,000 *g*, 1 h, 4 °C). For the characterization of drug release in the presence of RBCs, cells were removed by mild centrifugation (420 *g*, 5 min) before the ultracentrifugation step.

*2.3. Generation of iLPs*

Antibody (Ab) coupling to LPs was performed following established protocols [5,11]. Briefly, sulfhydryl groups were placed on Abs, either in primary amines or in aldehydes previously generated through sodium periodate ($NaIO_4$) oxidation of carbohydrates in the Ab Fc region, using the crosslinkers N-succinimidyl S-acetylthioacetate (SATA, Thermo Fisher Scientific, Inc.) or 3-(2-pyridyldithio)propionyl hydrazide (PDPH, Thermo Fisher Scientific, Inc.), respectively, for their subsequent conjugation to maleimide-containing LPs. Unconjugated Abs were removed by ultracentrifugation (150,000 *g*, 1 h, 4 °C) and pelleted iLPs were finally resuspended in isotonic PBS. Sterility was maintained throughout the coupling process by filtering all reagents through 0.22 μm pore size polyvinylidene difluoride filters (Millex-GV Syringe Filter Units, 4 mm, Millipore). Qualitative (sodium dodecyl sulfate-polyacrylamide gel electrophoresis, SDS-PAGE) and quantitative (QuickStart™ Bradford Protein Assay, Bio-Rad) antibody coupling analysis, along with the number of bound Ab molecules per LP, was assessed in accordance with previously standardized methods [5,11]. A typical qualitative SDS-PAGE analysis is presented in Fig. S1.

*2.4. Quantification of drugs and fluorescent dyes in LP samples*

Encapsulated drugs were quantified by disrupting LPs through addition of 0.1 vol of 10% w/v SDS, followed by 10 min bath sonication at 60 °C. UV spectra were subsequently obtained from 2 μl of detergent-treated samples using an Epoch™ spectrophotometer (BioTek Instruments, Inc., Winooski, VT, USA) in Take3 mode. Drug standards for quantification were prepared in either RPMI-A (plus 10 min water bath sonication at 60 °C) or PBS depending on their lipophilic or hydrophilic nature, respectively. Empty SDS-treated LPs and drug solvents were used as blank controls for absorbance subtraction. Standard curves for drug quantification were finally obtained by linear/quadratic regression from at least 3 independent measurements.

For rhodamine quantification in human and mouse RBC samples incubated with iLPs, pelleted cells (700 *g*, 5 min) were taken up in RPMI-A and treated with one vol of 4% v/v Triton X-100 in PBS for sample homogenization. Fluorescence measurements (DOPE-Rho, λex/em = 530/590 nm) were done in a Synergy HT Multi-Mode Microplate Reader (BioTek Instruments, Inc.). Known amounts of LPs diluted in the same matrix as the samples analyzed (i.e. RBC-containing RPMI-A and plasma obtained from untreated mice) were used as standards for quantification. *In vitro* liposome retention was expressed as the percentage of LPs within the RBC pellet fraction relative to the total amount present in the sample. Liposome blood clearance was determined by calculating the percentage of LPs in circulation (in RBC pellet plus plasma fractions) at a given time relative to the total liposome payload initially injected (i.e. 2 min post-administration, $t_0$). Blood biodistribution of LPs at specific post-administration times was determined by comparing the corresponding liposome concentrations within RBC pellet vs. blood plasma fractions.

### *2.5. Assessment of the antimalarial activity of drugs preloaded into non-infected erythrocytes*

All human blood samples used for *P. falciparum in vitro* cultures were purchased from the Banc de Sang i Teixits (http://www.bancsang.net/) and irreversibly anonymized prior to their arrival. Blood group B human RBCs suspended at 6% hematocrit in RPMI-A were diluted with one vol of 2× concentrated drugs in RPMI-A and the mixture was incubated for 24 h at 37 °C. Drug-containing cells were subsequently spun down (700 *g*, 5 min) and taken up in fresh RPMI-A prior to the addition of pRBCs in order to obtain final parasitemia and hematocrit of 0.5% and 3.3%, respectively. Non-washed cells containing full drug dosages and similarly mixed with pRBCs were included as positive control. Parasite growth inhibition was finally assessed as described below.

### *2.6. P. falciparum in vitro culture and growth inhibition assays*

*P. falciparum* strains 3D7 (CQ-sensitive) and W2mef (CQ-resistant) were cultivated in blood group B human RBCs according to standard protocols [46]. Synchronized cultures in early ring stages (0-24 h post-invasion) were obtained by 5% sorbitol lysis [47]. Late-form trophozoite and schizont stages (24-36 h and 36-48 h post-invasion, respectively) were purified in 70% Percoll (GE Healthcare) [48]. Parasitemia was determined by microscopic counting of blood smears fixed briefly with

methanol and stained with Giemsa diluted 1:10 in Sorenson's buffer, pH 7.2, for 10 min. For culture maintenance, parasitemia was kept below 5% late forms and 10% early forms by dilution with freshly washed RBCs and the medium was changed every 1-2 days. *In vitro* growth inhibition assays were conducted using synchronized *P. falciparum* cultures (>95%) in early or late form stages at 4% hematocrit and 1% parasitemia as previously described [11]. Unless otherwise specified, one culture volume of 2× concentrated drug solution in RPMI-A was added to the parasitized cell suspension and the mixture was incubated under orbital stirring for 15 min in 2-ml Petri dishes. The cells were finally transferred to microcentrifuge tubes and spun down, replacing the medium with fresh RPMI-A. The resulting cell suspension was then seeded on 96-well plates and further incubated for a complete 48-h growth cycle under the conditions described above. For the determination of parasite growth inhibition, samples were diluted 1:100 in isotonic PBS, and the nuclei of pRBCs (the only nucleated cells present in the culture) were stained by addition of 0.1 μM Syto11 (Thermo Fisher Scientific, Inc.) in the final mixture before proceeding to flow cytometry analysis. Growth inhibition in drug-treated samples was defined as the percentage decrease in parasitemia within the second generation of parasites relative to untreated control samples exhibiting complete parasite growth and multiplication. Drug IC50 corresponds to the concentration leading to 50% parasite growth inhibition relative to an untreated control culture.

*2.7. Flow cytometry*

For *Plasmodium* growth inhibition determination and quantitative live cell targeting examination of LPs, samples were analyzed at 0.02% hematocrit in PBS with a BD LSRFortessa™ cell analyzer (Becton, Dickinson and Company, New Jersey, USA). Forward- and side-scatter areas (FSC-A, SSC-A) in a linear scale were used to gate the RBC population, and pRBCs stained with either Syto11 or Hoechst 33342 fluorescent dyes were detected, respectively, by excitation through a 488 or 405 nm laser and emission collection with a 525/50 or 450/50 (Pacific Blue-A) nm bandpass filter in a logarithmic scale. pRBCs targeted by immunoliposomes incorporating in their formulation the rhodamine-conjugated lipid DOPE-Rho were detected by excitation through a 561 nm laser and emission collection with a 610/20 nm bandpass filter in a logarithmic scale (PE-YG-A). Acquisition was configured to stop after recording 20,000 events within the RBC population. Parasitized erythrocytes in late forms were discerned from those in early stages by their increased Hoechst 33342 or Syto11 signal, resulting from the presence of segmented parasites with multiple nuclei. RBC

agglutinates were determined after incubation with iLPs by counting those cell disproportion events in FSC height-area (H-A) confronted parameters, which indicated the presence of cell doublets as previously described in [11]. Agglutination rate (%) is expressed as the fraction of RBCs forming aggregates relative to the total number of erythrocytes present in the sample.

*2.8. Fluorescence microscopy*

For fluorescence assays with live cells of the targeting efficiency of iLPs, *in vitro* RBC suspensions (either blood group B human RBCs or BALB/c mouse RBCs collected in 0.2% w/v EDTA) were brought to 4% hematocrit and washed twice (700 *g*, 5 min) in RPMI-A before their incubation with one volume of 2× concentrated iLP samples under orbital stirring. Unless otherwise indicated, after 30 min of iLP-RBC incubation, cells were diluted to 0.1% hematocrit in PBS supplemented with 0.75% w/v bovine serum albumin (PBS-BSA) and finally deposited onto Lab-Tek™ chambered coverglass slides (Thermo Fisher Scientific, Inc.). Microscopic analysis was done with an Olympus IX51 inverted system microscope equipped with an IX2-SFR X–Y stage, a U-TVIX-2 camera, and a fluorescence mirror unit cassette for UV/blue/green excitation and detection of the corresponding blue/green/red emission ranges. Phase contrast images were acquired simultaneously. When evaluating iLP performance *in vivo* in *P. yoelii* 17XL-infected mice, blood was collected at specific post-administration times in 0.2% w/v EDTA or heparinized tubes when analyzing large (mouse facial vein) or small (terminal portion of animal tail) sample volumes, respectively. pRBC nuclei were stained with 2 µg/ml Hoechst 33342 and cells were finally diluted 1:200 v/v in PBS-BSA prior to fluorescence microscopy analysis as described above.

*2.9. Maximum tolerated dose (MTD) assay*

All experiments involving mice were performed in accordance with the corresponding relevant guidelines and regulations. The studies reported here were performed under protocols reviewed and approved by the Ethical Committee on Clinical Research from the Hospital Clínic de Barcelona (Reg. HCB/2014/0910). The animal care and use protocols followed adhered to the specific national and international guidelines specified in the Spanish Royal Decree 53/2013, which is based on the European regulation 2010/63/UE. Inbred BALB/c mice were individually monitored during 8 days following an analogous drug dosage regime to the *in vivo* assays performed in this work. In the presence of toxic effects including, among others,

>20% reduction in animal weight, aggressive and unexpected animal behavior or the presence of blood in defecations, animals were immediately anesthetized using a 100 mg/kg Ketolar plus 5 mg/kg Midazolan mixture and sacrificed by cervical dislocation. Drug MTD was therefore defined upon completion of the assay as the highest dosage exhibiting an absence of the aforesaid toxicity signs.

### *2.10. Determination of P. yoelii 17XL growth inhibition in mice*

*Plasmodium* growth inhibition *in vivo* was assessed in immunocompetent female BALB/c mice infected with the *P. yoelii* 17XL lethal strain after following daily treatment courses with antimalarial drugs and according to protocols previously established [37]. Briefly, 2-3 hours prior to starting drug treatment (day 0), healthy mice were intraperitoneally administered $2 \times 10^7$ parasitized erythrocytes from an already infected mouse. Each of 3 animal replicates per sample subsequently received daily drug dosages administered either intraperitoneally or intravenously (i.v.). *P. yoelii* 17XL-infected mice injected with drug solvents (untreated mice) were included for determination of the maximum parasite replication rate. Parasitemia was monitored daily from day 0 by microscopic examination. Antimalarial activity of the compounds studied in this work is expressed in terms of daily reductions in the parasite replication rate as well as of the overall growth inhibition, the latter being determined the day after completing drug administrations and expressed as the reduction of parasitemia percentage in treated mice relative to control untreated animals exhibiting maximum parasite growth and replication.

## 3. Results and Discussion

### *3.1. Selection of antimalarial drugs and characterization of their interaction with RBCs*

Considering the major goals of this RBC-targeted immunoliposomal approach (transporting amphiphilic/lipophilic compounds and displaying a simultaneous therapeutic/prophylactic antimalarial activity), the capacity of several antimalarial drugs to become internalized and retained into RBCs for their later inhibition of *P. falciparum* growth was first assayed *in vitro*. The antiplasmodial agents studied here belong to the 4-aminoquinoline (CQ and its derivatives 7c and 7d), 8-aminoquinoline (primaquine and tafenoquine), aminoalcohol (quinine, BCN-01 and BCN-02), and 9-aminoacridine (quinacrine) drug classes (Fig. 1). These compounds were selected on the basis of: (i) the presence of weakly basic groups undergoing protonation in the pH range 4.0-7.4, a

property which is required for active encapsulation in liposomes keeping a pH gradient; (ii) adequate molecular dimensions in order to avoid causing structural deformations when inserted into the liposome membrane; and (iii) their hydrophobic nature, feature represented by the octanol/water partition coefficient or log *P* (Table 1). 7c and 7d had been formerly reported to display potent *in vitro* activity against blood stages of CQ-sensitive and CQ-resistant *P. falciparum* strains, while being unable to exhibit such antimalarial potency *in vivo* when in free form [13]. The antiplasmodial activity of aminoalcohols BCN-01 and BCN-02 had been validated *in vitro* against both CQ-sensitive and multidrug-resistant *P. falciparum* strains and *in vivo* using the *P. berghei* murine malaria model [12], although this parasite species displays a reticulocyte-prone infective tropism similar to that of *Plasmodium vivax* human malaria, which significantly differs from *P. falciparum* pathophysiology.

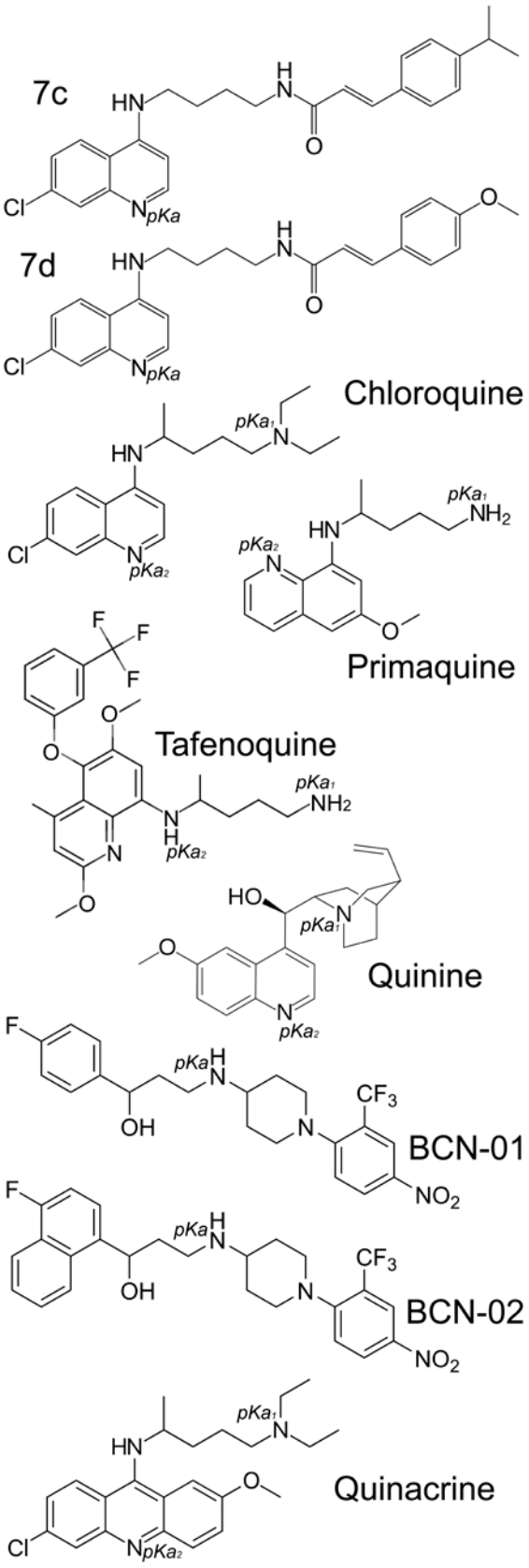


**Fig. 1.** Un-ionized molecular structures of the antimalarial compounds studied in this work. The corresponding pKas are indicated in Table 1.

**Table 1**

Description of the compounds assayed in this work. pKa and log *P* values were obtained from the Chemicalize software developed by ChemAxon Ltd [44], except for CQ [49] and primaquine [50]. pKa, $pKa_{1/2}$: pKas indicated in Fig. 1, which correspond to groups that become ionized in the pH gradient of the liposomal system used here (4.0-7.4). *M*r: relative molecular mass.

| Drug | Family | *M*r | Molecular formula | pKa, $pKa_{1/2}$ | log *P* | Solvent |
|---|---|---|---|---|---|---|
| Quinine | Aminoalcohol | 324.42 | $C_{20}H_{24}N_2O_2$ | 9.05/4.02 | 2.51 | Methanol |
| BCN-01 | Aminoalcohol | 477.88 | $C_{21}H_{23}F_4N_3O_3 \cdot HCl$ | 9.78 | 3.84 | Methanol |
| BCN-02 | Aminoalcohol | 491.48 | $C_{25}H_{25}F_4N_3O_3$ | 9.77 | 4.83 | Methanol |
| Chloroquine | 4-aminoquinoline | 515.86 | $C_{18}H_{26}ClN_3 \cdot 2H_3PO_4$ | 10.2/8.4 | 4.72 | $H_2O$ |
| 7c | 4-aminoquinoline | 421.97 | $C_{25}H_{28}ClN_3O$ | 7.31 | 5.41 | Methanol |
| 7d | 4-aminoquinoline | 409.91 | $C_{23}H_{24}ClN_3O_2$ | 7.31 | 4.01 | Methanol |
| Primaquine | 8-aminoquinoline | 455.34 | $C_{15}H_{21}N_3O \cdot 2H_3PO_4$ | 10.4/3.2 | 3.20 | $H_2O$ |
| Tafenoquine | 8-aminoquinoline | 581.58 | $C_{24}H_{28}F_3N_3O_3 \cdot C_4H_6O_4$ | 10.2/3.2 | 4.97 | Methanol |
| Quinacrine | 9-aminoacridine | 472.88 | $C_{23}H_{30}ClN_3O \cdot 2HCl$ | 10.33/8.37 | 5.15 | $H_2O$ |

The antimalarial prophylactic activity of all compounds included in this work was assessed in a three-step process: (i) initial 24 h incubation with human RBCs to maximize drug partition and internalization into the cells; (ii) washing of RBCs to remove non-incorporated drug prior to infection with *P. falciparum* at two different metabolic stages in the intraerythrocytic parasite cycle: ring (early) and trophozoite/schizont (late) forms; and (iii) parasite growth finally measured after a 48 h replication cycle. Most antimalarials exhibited non-significant differences in their activity when comparing washed vs. non-washed RBCs regardless of the parasite stage (Figs. S2 and S3; Tables 2 and S1), which reflected their lipophilic character and thus their affinity for RBC plasma membranes. Significant differences were only obtained for quinine (compound presenting the lowest log *P*, 2.51 units), and the highly protonated antimalarial CQ (pKas 8.4 and 10.2). For subsequent encapsulation assays in targeted immunoliposomes, four drugs were selected on the basis of their novelty and/or high antimalarial activity, namely BCN-02, 7c, quinacrine and CQ.

**Table 2**

*P. falciparum* growth inhibition assays in parasite cultures at either ring (early) or late forms. The results are expressed as parasite growth IC50 (nM) after drug internalization into RBCs (washed RBCs), compared to non-washed RBC samples in which excess of antimalarials was not removed. IC50 values were calculated considering the initially added drug concentrations. Included in the table are the corresponding washed vs. non-washed IC50 fold change rates along with their related *p* values calculated using $\log_{10}$(IC50) values (Table S1). NA: not analyzable.

| | IC50 (nM) | | | |
|---|---|---|---|---|
| | Washed RBCs | Non-washed RBCs | Fold change | *p* value |
| | | Rings | | |
| Quinine | 2303.0 | 438.0 | 5.3 | $3.3\times10^{-3}$ |
| BCN-01 | 4393.0 | 3574.0 | 1.2 | 0.39 |
| BCN-02 | 508.9 | 334.3 | 1.5 | 0.09 |
| Chloroquine | 162.8 | 50.4 | 3.2 | $1.4\times10^{-3}$ |
| 7c | 5888.4 | 1047.1 | 5.6 | 0.73 |
| 7d | NA | 3715.4 | NA | NA |
| Primaquine | NA | ~10000 | NA | NA |
| Tafenoquine | 9066.0 | 4298.0 | 2.1 | 0.87 |
| Quinacrine | 56.2 | 21.9 | 2.6 | 0.55 |
| | | Late forms | | |
| Quinine | 2350.0 | 478.8 | 4.9 | 0.01 |
| BCN-01 | 4307.0 | 2663.0 | 1.6 | 0.10 |
| BCN-02 | 454.9 | 350.2 | 1.3 | 0.48 |
| Chloroquine | 162.3 | 17.8 | 9.1 | 0.03 |
| 7c | 1513.6 | 138.0 | 11.0 | 0.22 |
| 7d | 1148.2 | 128.8 | 8.9 | 0.35 |
| Primaquine | NA | 8511.4 | NA | NA |
| Tafenoquine | NA | 3020.0 | NA | NA |
| Quinacrine | 44.7 | 14.5 | 3.1 | 0.26 |

*3.2. Analysis of the encapsulation efficiency into liposomes of the selected compounds*

The capacity of the selected lipophilic antimalarials BCN-02 and 7c to become actively encapsulated into LPs using a citrate/phosphate-buffered pH gradient system was determined. Because these compounds must be prepared in organic solvents and incorporated into the lipid mixture during LP preparation, their interaction with LPs at pH 4.0 and their subsequent retention upon formation of the pH gradient was first analyzed through a buffer exchange process. Drug-nanoparticle interaction in acidic conditions was evaluated by measuring LP ζ-potential (Table S2). Both BCN-02 and 7c induced large LP surface charge modifications when compared to the drug-free control LP sample due to their strong hydrophobicity of 4.8 and 5.4 log *P* units, respectively (Table 1). Furthermore, BCN-02 imparted a higher nanoparticle surface charge in

comparison to 7c most likely because of its more ionizable basic group (respective pKas of 9.8 and 7.3). Remarkably, an absence of LP surface charge alteration relative to drug-free LPs used in this work as negative control was observed after buffer exchange, indicating effective drug internalization.

A method for the rapid UV/visible spectral quantification of LP-encapsulated cargo was developed to determine the amounts of the antimalarial compounds under study throughout the internalization process and in the presence of liposome components. Briefly, solutions containing LPs actively loaded with the four selected drugs were treated with 1% SDS and sonicated for a few minutes to disrupt LP particles while solubilizing drugs within detergent micelles. Neither liposome components nor SDS caused interferences in absorption spectra of the drugs after treatment (Figs. S4 and S5). In accordance with LP surface ζ-potential data, BCN-02 was better retained than 7c after the buffer exchange step (ca. 75% vs. 60%, respectively, of total drug initially present in the citrate-solubilized lipid mixture; Table 3).

**Table 3**

Analysis of active drug encapsulation into LPs through a citrate/phosphate-buffered pH gradient. Drug concentration was determined by UV/vis spectroscopy (Figs. S4 and S5) after each step of the process including (i) initial LP formation in citrate buffer (LPs citrate; here the lipophilic compounds 7c and BCN were incorporated), (ii) buffer exchange (BE) with PBS (LPs post-BE; here the water-soluble CQ and quinacrine were added to preformed LPs), and (iii) ultracentrifugation of samples in PBS (LPs post-ultra) to determine encapsulated drug at the end of the process. The volumes of all samples were kept equal for a straightforward reading of drug concentrations. EE: encapsulation efficiency.

| | Drug (μM), mean ± SD | EE (%), mean ± SD |
|---|---|---|
| | BCN-02 | |
| LPs citrate | 221.3 ± 1.5 | - |
| LPs post-BE | 165.2 ± 4.9 | 74.7 ± 2.2 |
| LPs post-ultra | 169.8 ± 8.1 | 102.8 ± 4.9 |
| | 7c | |
| LPs citrate | 205.5 ± 19.3 | - |
| LPs post-BE | 121.9 ± 19.4 | 59.0 ± 5.3 |
| LPs post-ultra | 107.7 ± 17.8 | 90.5 ± 5.4 |
| | Chloroquine | |
| LPs post-BE + Drug | 225.1 ± 6.0 | - |
| LPs post-ultra | 206.3 ± 4.7 | 91.6 ± 2.1 |
| | Quinacrine | |
| LPs post-BE + Drug | 234.0 ± 1.8 | - |

| | | |
|---|---|---|
| LPs post-ultra | 223.0 ± 3.2 | 95.3 ± 1.4 |

All compounds were quantitatively retained with more than 90% drug remaining stably internalized after ultracentrifugation of phosphate buffer-exchanged LP samples. Remarkable retention efficiency was maintained up to 30 days in storage conditions (Fig. S6A). A significant increase of released drug amounts was observed under *in vitro* culture conditions, especially in the presence of RBCs (Fig. S6B,C). The lipophilic compounds BCN-02 and 7c exhibited the largest cumulative release yields of ca. 20-30% after 30 min incubation in the presence of cells (Fig. S6C), presumably due to the existence of lipid exchange mechanisms taking place between LPs and plasma membranes, as theorized in previous works [5,51]. Alternatively, sustained release processes driven by temperature and dilution-dependent depletion of the proton gradient across LP membranes [11] might be hypothesized for the leak of the hydrophilic compounds CQ and quinacrine from LPs, which accounted for ~20% release yields after 6 h incubation with RBCs (Fig. S6C). Drug internalization into RBCs would be explained in this case by passive diffusion of released un-ionized molecules across lipid bilayers.

*3.3. Immunoliposome targeting to mouse RBCs*

The conjugation of LPs with the TER-119 monoclonal Ab (TER119-iLP model), specific for a 52 kDa RBC surface antigen characteristic of the murine erythroid lineage and specifically expressed from the early proerythroblast to mature RBC stages [52,53], was optimized in order to design a RBC-targeted nanoparticle to be used in immunocompetent mice. In parallel, the coupling of LPs with the monoclonal mouse anti-human GPA Ab (GPA-iLP model, [11]) was improved for the reduction of agglutinating events *in vitro* during the performance of *Plasmodium* growth inhibition assays. iLP generation was based on the conjugation of freshly prepared maleimide-containing LPs with thiolated antibodies. Sulfhydryl groups were introduced through two distinct approaches: (i) derivatization of Ab primary amines with the SATA crosslinking agent was used for both anti-GPA- and TER119-iLP models with an Ab:LP ratio of 0.1 to 1 mg Ab/ml of 10 mM lipid (i.e. 10-100 µg Ab/µmol lipid; for simplicity, the Ab/lipid ratio used in iLP preparation will be hereafter expressed as µg Ab/µmol lipid). Different SATA:Ab molar ratios (10× to 2×) were analyzed for TER-119 conjugation in order to explore the potential loss in antigen recognition due to modification of primary amines in the vicinity of the antigen-binding site. (ii) Oriented TER-119 coupling to

liposomes through the carbohydrate moiety in Ab Fc regions was studied comparing two different degrees of carbohydrate oxidation using 10 and 5 mM $NaIO_4$. Efficiency of anti-GPA and TER-119 antibody conjugation to liposomes was finally evaluated *in vitro* as the capacity of the resulting iLPs to target human and mouse erythrocytes, respectively.

Using 10× SATA:Ab, small differences in the percentage of targeted cells (Fig. 2A) and in the amount of RBC-retained GPA-iLPs (Fig. 2B) were observed above 50 µg Ab/µmol lipid, but at lower Ab:LP ratios GPA-iLP binding efficacy to target cells significantly decreased, as evidenced by the fall in the fraction of retained iLPs. A considerable reduction in GPA-iLP-mediated RBC agglutination from more than 40% to ~27% at 100 µM lipid was obtained when decreasing the antibody concentration during iLP preparation from 100 to 50 µg Ab/µmol lipid, respectively (Fig. 2A), and an absence of agglutinates was observed at 10 µM lipid for ≤50 µg Ab/µmol lipid (Fig. 2C). Based on these data, for subsequent experiments 50 µg Ab/µmol lipid and 10× SATA:Ab were therefore selected, which resulted in 111 ± 8 Ab molecules per LP.

LP conjugation with TER-119 through Ab primary amines using 10× SATA:Ab resulted in iLPs exhibiting an almost complete RBC targeting above 10 µM lipid (Figs. 2D and S7), albeit with most iLPs not retained onto cells even at a conjugation ratio of 100 µg Ab/µmol lipid (Fig. 2E). The same Ab concentration but using 5× and 2× crosslinker amounts improved respective iLP retention yields to about 30-40% and 10-30% and also increased cell targeting rates and minimized agglutination (Fig. 2D). This improvement obtained at smaller SATA:Ab molecular ratios likely reflected interferences in antigen recognition upon excessive TER-119 primary amine modification. An almost complete retention onto RBCs was achieved by means of increasing the incubation time from 30 min to 3 h and doubling the amount of cells during incubation from 2 to 4% hematocrit (Fig. S8). In comparison, conjugation of equal amounts of antibodies through carbohydrate moieties exhibited slightly lower retention capacity (≤20%; Fig. 2E) regardless of the TER-119 oxidation state. Because of the lack of agglutination observed up to 50 µM lipid (where a 100% RBC targeting was achieved) for TER-119 conjugated to liposomes using 5× SATA:Ab at 100 µg Ab/µmol lipid (Figs. 2D and S9), these settings (resulting in 133 ± 11 Ab molecules per LP) were selected for *in vivo* assays.

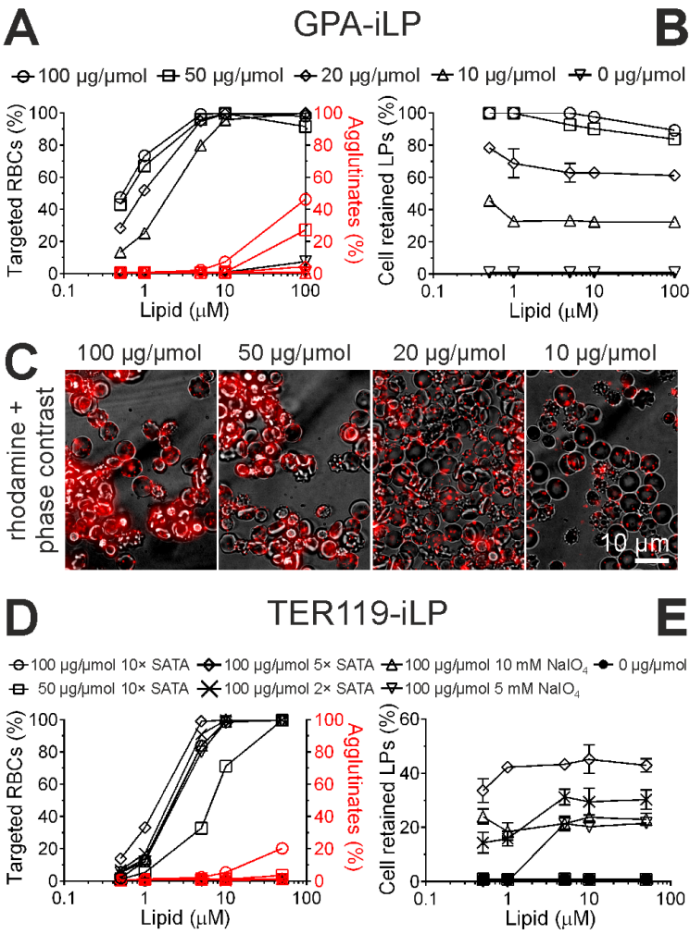


**Fig. 2**. Optimization of RBC-specific monoclonal antibody coupling to LPs. (A-C) Analysis of anti-GPA Ab conjugation efficacy through primary amines (using 10× SATA:Ab and 10 to 100 µg Ab/µmol lipid during the conjugation reaction), represented as percentage (A) of targeted and agglutinated human RBCs and (B) of retained LPs after 30 min incubation. (C) Fluorescence microscopy images of the 10 µM lipid samples from panel A. (D,E) Analysis of TER-119 Ab conjugation efficacy through either primary amines at different SATA:Ab ratios or carbohydrate moieties with different degrees of oxidation (5 or 10 mM $NaIO_4$), using 50 or 100 µg Ab/µmol lipid; the data are represented as percentage (D) of targeted and agglutinated mouse RBCs and (E) of retained LPs after 30 min incubation.

### *3.4. In vitro P. falciparum growth inhibition activity of iLP-encapsulated drugs*

To choose the best iLP-encapsulated drug (iLP[drug]) candidates for *in vivo* assays, the antimalarial activity of the drugs actively encapsulated in the GPA-iLP nanocarrier was assayed *in vitro* in *P. falciparum* cultures of the 3D7 strain. After only 15 min incubation with parasite cultures at both early and late stages, immunoliposomal encapsulation provided a significant decrease in drug IC50 values

when compared to the same amounts administered in free form (Fig. 3). BCN-02 and 7c offered the best improvement in growth inhibition activity upon encapsulation, with respective iLP[drug] vs. free drug IC50 fold change units obtained when administered to early/late parasitic forms of 14.8/12.8 for 7c and of 5.7/5.6 for BCN-02 (Tables 4 and S3). Remarkably, the GPA-iLP-encapsulated CQ structural analogue 7c (GPA-iLP[7c]) was even more effective against the CQ-resistant W2mef *P. falciparum* strain when administered to late forms, leading to a 26.4 IC50 fold change vs. free 7c, with an absolute IC50 around half that obtained with 3D7 (48.6 vs. 100.7 nM, respectively). On the other hand, a similar enhancement upon encapsulation of CQ antiparasitic efficacy was obtained in both 3D7 and W2mef, although requiring in the latter case significantly larger drug amounts.

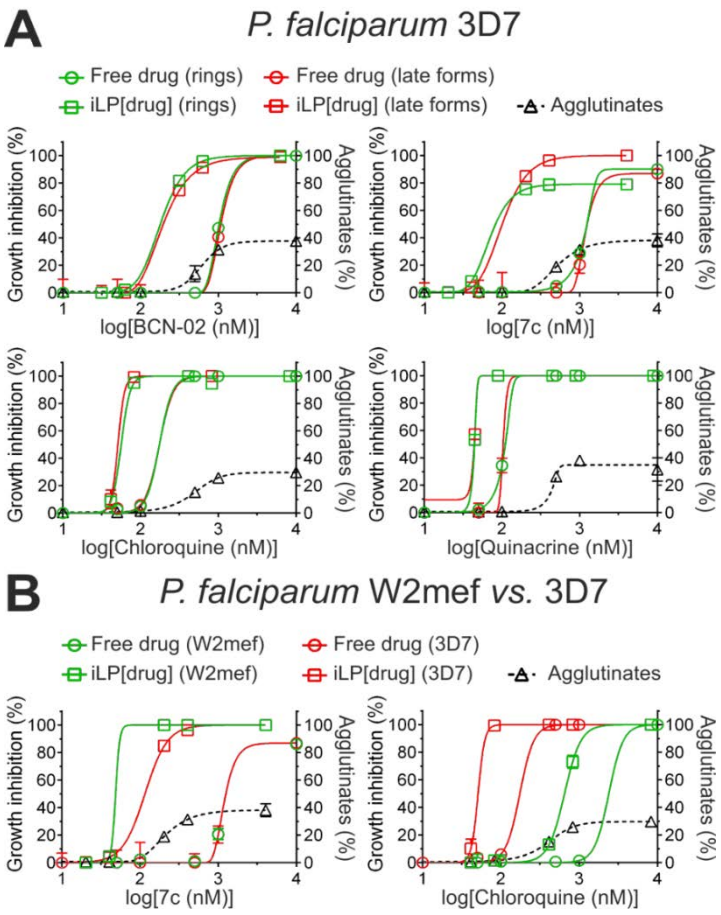


**Fig. 3**. *In vitro P. falciparum* growth inhibition assays. GPA-iLP-encapsulated vs. freely delivered antimalarials were added to parasite cultures at either ring or late stages and removed after 15 min; parasitemia was determined after 48 h of incubation. (A) Analysis of BCN-02, 7c, CQ and quinacrine with the *P. falciparum* 3D7 strain. (B) Comparative analysis of 7c and CQ added at late stages to 3D7 and to the CQ-resistant W2mef *P. falciparum* strain.

**Table 4**. Analysis of the data from Fig. 3. Results are expressed as parasite growth IC50 (nM) and the corresponding free drug vs. GPA-iLP[drug] IC50 fold change. *p* values were calculated using $\log_{10}$(IC50) values (Table S3).

| | IC50 (nM) | | | |
|---|---|---|---|---|
| | Free drug | GPA-iLP[drug] | Fold change | *p* value |
| | | Rings (3D7) | | |
| BCN-02 | 1021.0 | 178.6 | 5.7 | $<1 \times 10^{-4}$ |
| 7c | 1230.3 | 83.2 | 14.8 | $<1 \times 10^{-4}$ |
| Chloroquine | 174.5 | 56.3 | 3.1 | $9 \times 10^{-4}$ |
| Quinacrine | 110.6 | 44.3 | 2.5 | $<1 \times 10^{-4}$ |
| | | Late forms (3D7) | | |
| BCN-02 | 1076.0 | 192.9 | 5.6 | $<1 \times 10^{-4}$ |
| 7c | 1288.2 | 100.7 | 12.8 | $<1 \times 10^{-4}$ |
| Chloroquine | 174.5 | 51.1 | 3.4 | $1 \times 10^{-3}$ |
| Quinacrine | 103.5 | 44.4 | 2.3 | $<1 \times 10^{-4}$ |
| | | Late forms (W2mef) | | |
| 7c | 1281.5 | 48.6 | 26.4 | $<1 \times 10^{-4}$ |
| Chloroquine | 2392.0 | 649.7 | 3.7 | 0.01 |

*3.5. MTD and pharmacokinetic analysis of 7c and BCN-02*

Mouse administration regimes were determined for the lipophilic compounds 7c and BCN-02, which displayed the highest *in vitro* antiparasitic activity improvements after their encapsulation in GPA-iLPs. The MTD for 7c had been previously established to be around 30 mg/kg [13]. A higher toxicity (MTD of 10 mg/kg) was obtained after 4-day intraperitoneal administration of BCN-02 emulsified in 10% v/v chloroform/RPMI-A (Table S4). When intravenously delivered at ≥1 mg/kg in the same emulsification mixture, which when free of drug was well tolerated by mice, both compounds caused severe toxicity killing the animals within three days post-administration (Table S5).

The toxicity of BCN-02 and 7c was further explored after liposomization of the compounds. Upon i.v. administration, passively encapsulated 7c and BCN-02 were remarkably well tolerated up to 10 and 20 mg/kg, respectively (Table S6). The *in vivo* pharmacokinetic behavior of both compounds encapsulated in non-targeted LPs was evaluated in mice after one single 10 mg/kg i.v. injection, which corresponded to an initial lipid concentration in blood of ~5 mM at the start of the analysis (Fig. 4A). Liposome circulation half-lives of about 6 h were determined in accordance with previous assays [11], with ~90% LPs still in circulation 90 min after administration. The antimalarial activity of the liposomized drugs was finally examined in *P. yoelii* 17XL-infected mice following a 4-day i.v. dosage regimen, being parasitemias determined on

the day after completing the injections (Fig. 4B). Modest antimalarial effects below ca. 20% decrease in blood parasite load were observed between 1 and 10 mg/kg administrations, but a considerable 45-55% parasitemia reduction was obtained at 20 mg/kg for both 7c and BCN-02.

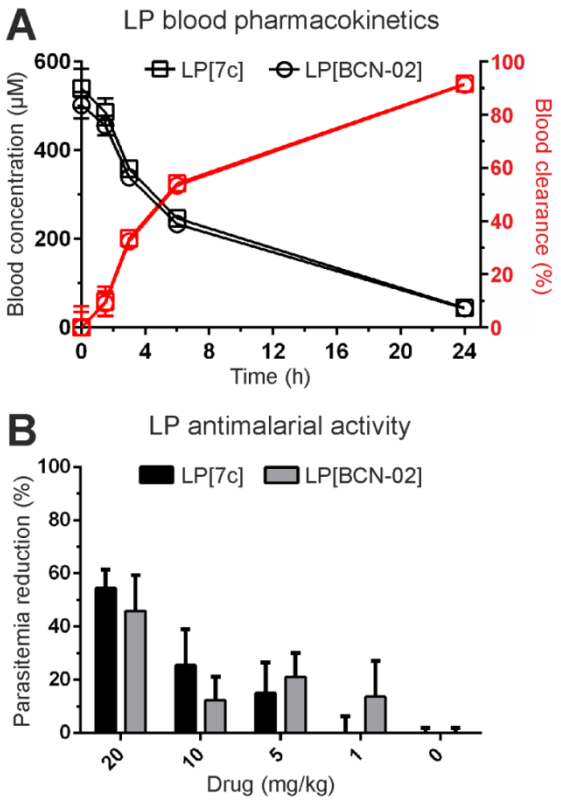


**Fig. 4.** *In vivo* pharmacokinetic analysis of 7c and BCN-02 administered i.v. and passively encapsulated in non-targeted liposomes. (A) Analysis of liposome residence in blood for 10 mg/kg drug dosage corresponding to a ca. 5 mM lipid concentration in circulation at the start of the analysis. (B) 4-day antimalarial assay in *P. yoelii* 17XL-infected mice after administration of 1 to 20 mg/kg liposomized drug dosages. Activity is expressed as the percentage of parasitemia reduction in comparison to untreated infected animals, determined one day after completing the administrations.

*3.6. Pharmacokinetic and blood biodistribution analysis of TER119-iLPs*

Possible effects of the different methods used for LP functionalization with TER-119 (primary amine vs. Fc carbohydrate crosslinking procedures) and dosage reduction on nanocarrier blood pharmacokinetics and plasma vs. RBC biodistribution were evaluated during 24 h after one single i.v. administration of iLPs devoid of drug. At an initial non-targeted LP blood concentration corresponding to ca. 125 μM lipid, a

considerable reduction in circulating LPs was observed 90 min after administration (~60% decrease relative to initially injected dose; Fig. 5A, LPs w/o Ab), a significantly larger removal rate than that previously obtained with a ca. 5 mM lipid dosage (Fig. 4A). More than 90% LP clearance from blood was completed 6 h after administration, with most liposomes being always localized in the plasma fraction (Fig. 5B). LP coupling with TER-119 moderately ameliorated the pharmacokinetic profile to about 40% and 80% iLP blood clearance at 1.5 and 6 h post-administration, respectively, with no remarkable differences observed due to the Ab conjugation technique followed. Over 80% TER119-iLPs were localized in the RBC fraction at $t_0$ (2 min post-administration), an efficient targeting which was maintained throughout the whole analysis, especially for primary amine conjugation using the 5× SATA:Ab ratio (Fig. 5B).

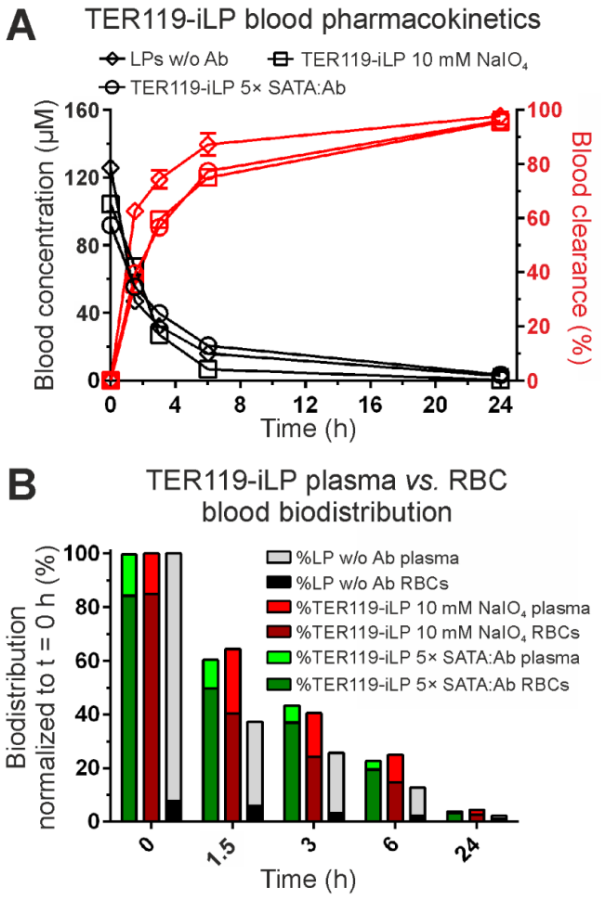


**Fig. 5.** Analysis of the effect on pharmacokinetic parameters of the TER119-iLP conjugation method (primary amines using 5× SATA:Ab vs. Fc carbohydrate oxidation with 10 mM $NaIO_4$). (A) Analysis of liposome residence in blood following an initial lipid concentration in circulation of ~125 μM. (B) Blood distribution analysis (circulating RBCs vs. plasma) of iLPs; non-targeted, Ab-free liposomes (LPs w/o Ab) are included for comparison.

*3.7. In vivo antimalarial activity in P. yoelii 17XL-infected immunocompetent mice of 7c encapsulated in TER119-iLPs*

The *in vivo* performance of the mouse RBC-targeted immunoliposomal approach optimized above, i.e. TER-119 conjugation to LPs via primary amine crosslinking using 5× SATA:Ab, was finally evaluated. Bearing in mind the requirement of a rapid *in vivo* performance because of the fast iLP blood clearance kinetics observed (Fig. 5A), 7c was selected as actively encapsulated drug cargo due to its lower ionization degree within the 4.0-7.4 pH range used when compared to BCN-02 (Fig. S10). The corresponding higher number of un-ionized drug molecules in TER119-iLPs will result in an increased capacity for this carrier of transferring drug to the targeted RBC/pRBC membrane before being cleared from blood. Additionally, a daily decreasing 5 to 1 mg/kg intravenous dosage regimen was established to avoid an excessive membrane saturation of circulating RBCs that might lead to undesired agglutination events.

BALB/c mice were initially infected with the murine malaria parasite *P. yoelii* 17XL lethal strain as immunocompetent model for human falciparum malaria, and parasitemias as well as the decrease in *Plasmodium* replication rate were followed daily by optical microscopy. Finally, all animals were exsanguined the day after completing i.v. administrations for the evaluation of the antimalarial activity of TER119-iLPs actively encapsulating 7c (TER119-iLP[7c]). Controls included infected mice either untreated or treated with 7c actively encapsulated in non-targeted liposomes (LP[7c]). Treatment with 7c in non-liposomal form was avoided because of its previously observed toxic effects *in vivo* above 1 mg/kg i.v. dose (Table S5). According to microscopic counts at the end of the assay, improved inhibition of *Plasmodium* growth was mediated by TER119-iLP[7c] in comparison to LP[7c]-treated and untreated mice, with respective parasitemias of 5.6 ± 1.0%, 26.0 ± 3.6% and 22.0 ± 5.6% (Fig. 6A). In addition, whereas an average daily parasite replication rate of 7- to 8-fold units was observed for both untreated and LP[7c]-treated mice, TER119-iLP[7c] administration resulted in a reduced replication rate of <3.5-fold units (Fig. 6B). Such differences in *P. yoelii* growth were more clearly reflected in the overall parasite replication rate (% parasitemia at day 3 vs. day 1) with 87.0 ± 11.0% averaged decrease when comparing TER119-iLP[7c]-treated (4.4 ± 1.1-fold units) vs. LP[7c]-treated and untreated mice (36.7 ± 3.6- and 31.1 ± 7.7-fold units, respectively).

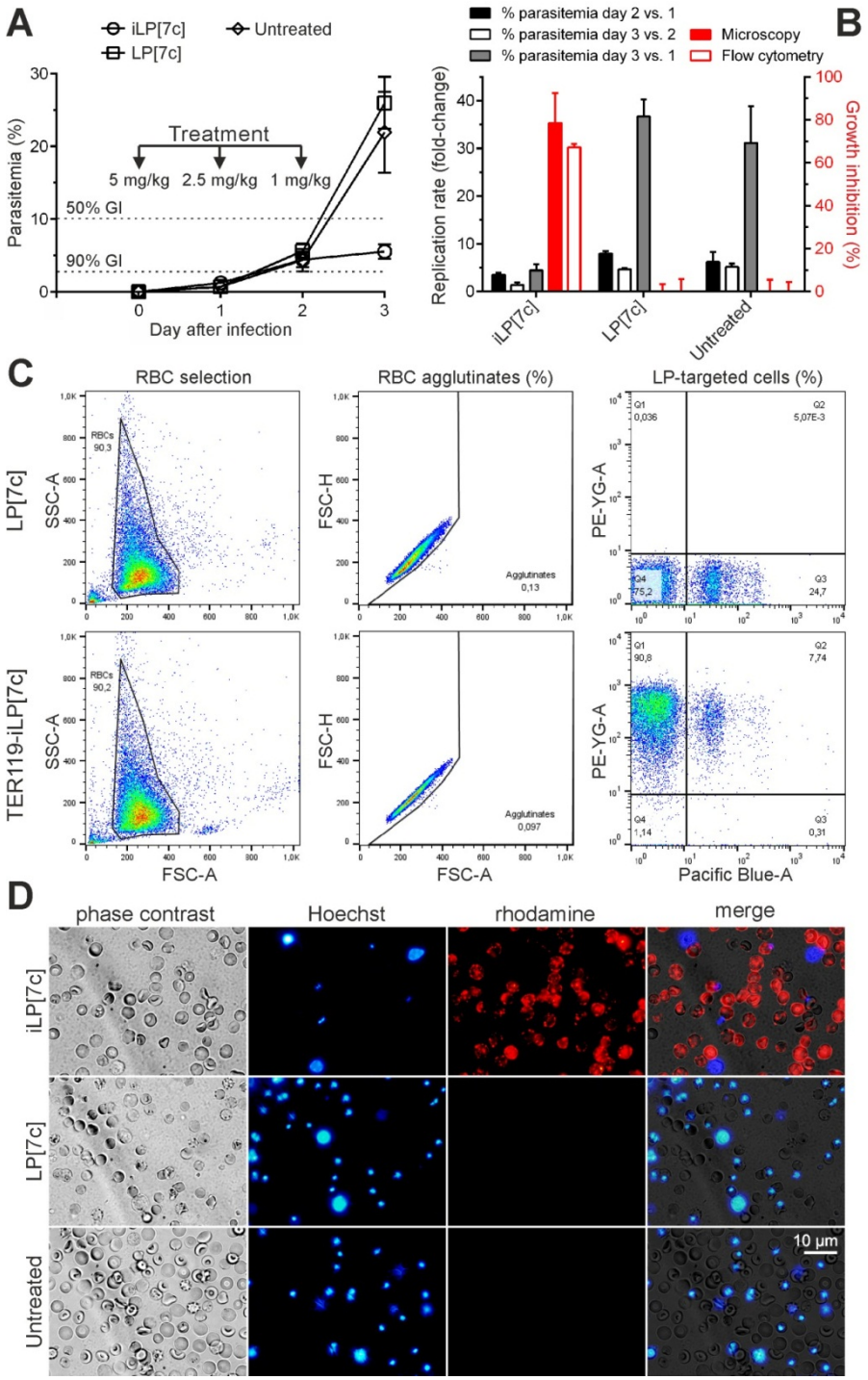


**Fig. 6.** *In vivo* study of the antimalarial performance of TER119-iLP[7c] (5× SATA:Ab) in *P. yoelii* 17XL-infected immunocompetent mice. (A) Microscopic daily determination of mice parasitemia. (B) Replication rates and growth inhibition of the parasite, the latter determined on day 3 post-infection by optical microscopy and flow cytometry. (C,D) Analysis on day 3 post-infection of LP[7c]- and TER119-iLP[7c]-treated mouse blood samples by (C) flow cytometry and (D) fluorescence microscopy. Pacific Blue-A and PE-YG channels are included in flow cytometry plots for the analysis of pRBC-nuclear and LP-associated rhodamine fluorescence signals, respectively.

Remarkably, LP[7c] administration caused no detectable effect on parasite development, whereas a final growth inhibition of 76.8 ± 13.4% was observed by optical microscopy examination following TER119-iLP[7c] administration (Fig. 6B). Flow cytometry analysis revealed a similar growth inhibitory effect of 70.6 ± 1.7%, as well as a good targeting efficacy for TER119-iLP[7c], with more than 95% [RBCs+pRBCs] resulting positive for rhodamine-iLP binding (Figs. 6C and S11). These results were qualitatively validated in parallel by fluorescence microscopy (Fig. 6D). However, whereas fluorescence-based techniques reported an absence of agglutinates on the day of analysis (Figs. 6C,D, and S11), slight reductions in mice weight of as much as 7.1% were observed after TER119-iLP treatment (Table S7), which might be indicative of potential side-effects at higher drug amounts than those assayed here.

## 4. Conclusion

In this work, we have successfully moved towards the validation of a RBC-targeted drug delivery system for severe falciparum malaria therapeutics applicable to several weakly basic antimalarials exhibiting distinct lipophilic and ionizable properties. The capacity of erythrocytes as drug carriers for novel antimalarial prophylactic strategies has been demonstrated by means of their efficient loading with compounds exhibiting poor water solubility and/or low ionization states at physiological pH. LP active encapsulation through the establishment of a citrate-buffered pH gradient allowed for the stable incorporation of hydrophobic drugs containing weakly basic ionizable moieties, which become principally localized into the inner LP membrane leaflet (Fig. 7). The aminoalcohol BCN-02 and the 4-aminoquinoline 7c were efficiently delivered into *P. falciparum*-infected RBCs upon encapsulation into erythrocyte-targeted immunoliposomes, inhibiting parasite growth *in vitro* and displaying significant improvements in drug activity when compared to free administered drug after only a 15-min exposure time to *P. falciparum* cultures. Best improvements in drug efficacy due to iLP-mediated delivery were furthermore obtained for the CQ analogue 7c when assayed in the CQ-resistant W2mef *P. falciparum* strain. The mechanism of action of heterocyclic-cinnamic conjugates to which 7c belongs has been proposed in previous works to be specific of *Plasmodium* metabolic routes. Namely, (i) impairment of the new permeation pathways formed by *Plasmodium* during its intraerythrocytic cycle and (ii) inhibition of β-hematin crystallization, process mediated by incorporating the CQ-analogous 4-aminoquinoline ring [13,43]. An absence of 7c toxicity against Huh7 human hepatoma cells was additionally reported in these works. Taken together, these

data suggest that 7c might be an interesting molecule for the future development of iLP-based antimalarial strategies.

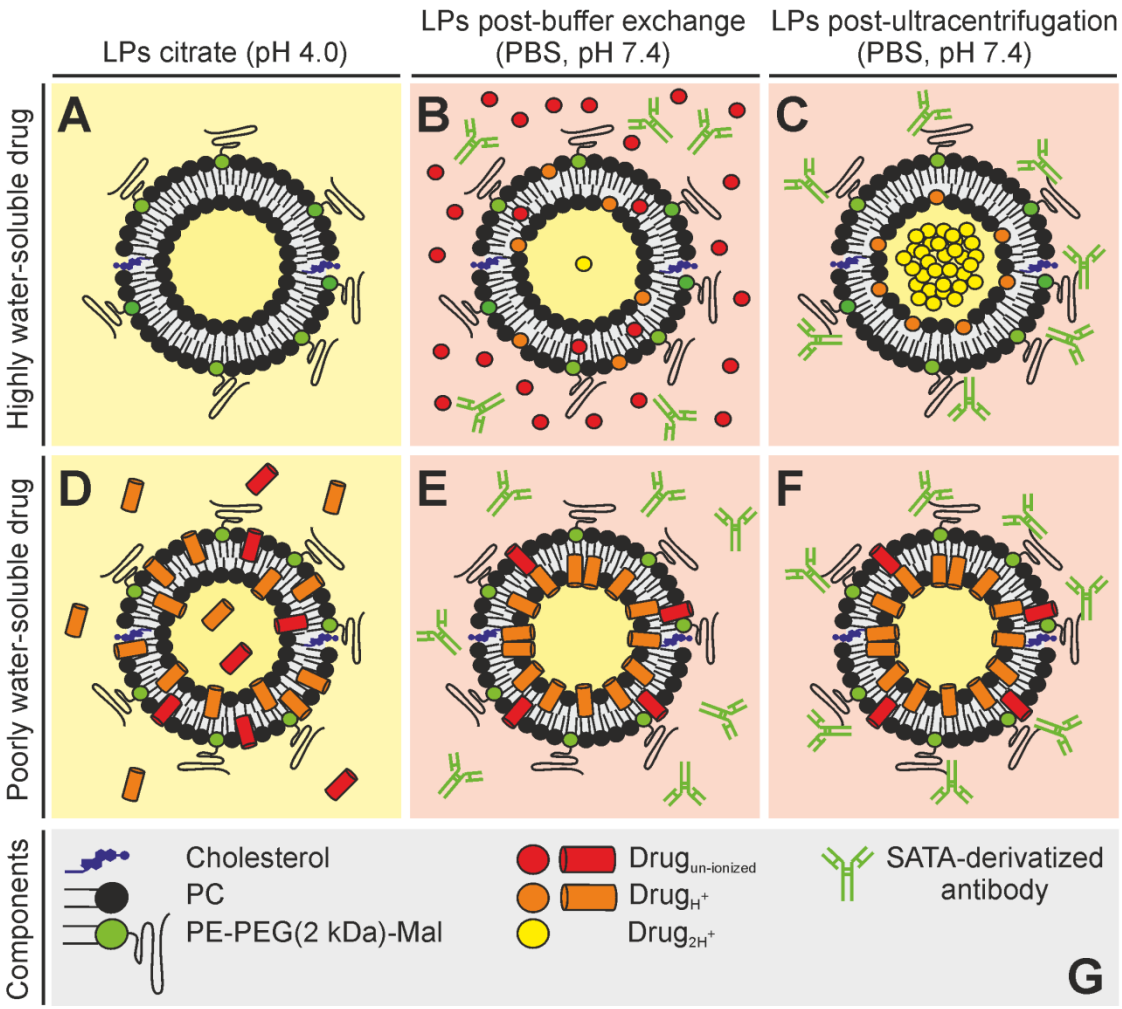


**Fig 7.** Citrate-buffered pH gradient systems assayed in this work for the active encapsulation in iLPs of hydrosoluble (CQ, quinacrine) and poorly water-soluble (7c, BCN-02) compounds used for *in vitro* and *in vivo* antimalarial assays. Key steps of the procedure include: (A,D) PC-based LP preparation containing maleimide-derivatized, PEGylated phospholipids in 200 mM citrate buffer, pH 4.0; (B,E) Buffer exchange of LP external solution to isotonic PBS, pH 7.4, containing SATA-derivatized thiolated antibodies; (C,F) final ultracentrifugation step to remove material not incorporated into iLPs. Hydrophilic drugs are added to LP samples at (B) the PBS buffer exchange step, whereas poorly water-soluble antimalarials are incorporated (D) in citrate solution during initial LP formation. (G) Summary of the main components used for iLP[drug] preparation.

Currently there is an urgent need to increase the repertoire of drugs available for severe malaria therapy, where intravenous administration of high drug amounts is usually required to rapidly clear *P. falciparum* infection. The RBC-targeted immunoliposome proposed here for lipophilic compounds fulfills these specifications, having a fast effect in reducing parasite levels. The antimalarial activity of this RBC-specific approach, previously assayed in humanized immunosuppressed mice using CQ as drug payload [11], has been validated in an immunocompetent and lethal murine malaria model similar to human blood infection by *P. falciparum*. The immunoliposomized 7c compound has been capable of reducing blood parasitemia down to uncomplicated levels (ca. 5%), whereas control animals treated with identical drug amounts encapsulated in non-targeted liposomes had parasitemias around 25%, a parasite load comparable to that found in severe stages of *P. falciparum* infection. In addition, the cost of humanized mice used in previous studies (ca. 2000 USD/animal) called for a more economically affordable strategy, especially considering the limited resources available for malaria research. The *P. yoelii* 17XL murine malaria model offers a cost-effective alternative for the *in vivo* study of immunoliposome-based severe malaria therapies.

Further optimization of the prototype presented here is required for progressing towards the clinical pipeline. Host immune responses against the injected particle that would result in fast drug clearance rates from circulation can be minimized using antibody fragments lacking the highly immunogenic Fc region and formulating liposomes with PEG-derivatized lipids for surface steric stabilization [54]. The iLP approach used here is specifically targeted towards the TER119 marker, which has been widely characterized and is specifically expressed from the early proerythroblast to mature mouse RBC stages. Although specific iLP interactions with circulating leucocytes are therefore not expected, the content of PEG-bearing lipids in the immunoliposomes used here (5%) can still be significantly increased if required to limit capture in the major lymphatic and blood filtering organs (spleen and liver) and uptake by the mononuclear phagocyte system [55]. Finally, reducing potential side effects derived from RBC agglutination due to the high hematocrit found in blood (approximately 40% v/v occupied by RBCs) can be successfully dealt with through a close control on the numbers of antibodies conjugated per liposome and on the amount of crosslinker agents used. The search for new erythrocyte surface targets displaying minimal agglutinating capacity should be also contemplated, especially if considering the encapsulation of compounds exhibiting low antimalarial efficacies *in vivo* [2,13], which will require larger liposome amounts in circulation.

**Acknowledgment**

This work was supported by: (i) grant BIO2014-52872-R from the Ministerio de Economía y Competitividad (MINECO), Spain, which included FEDER funds; (ii) grant 2014-SGR-938 from the Generalitat de Catalunya, Spain; (iii) PIUNA Project (Universidad de Navarra), and (iv) Foundation CAN (grant number: 70391). The authors are grateful to the Instituto de Salud Tropical (ISTUN) of Universidad de Navarra for the financial support and help. Thanks are due to Fundação para a Ciência e Tecnologia (FCT, Portugal) for funding research unit LAQV-REQUIMTE (ref. UID/QUI/50006/2013). Thanks are also due to "Comissão de Coordenação e Desenvolvimento Regional do Norte (CCDR-N)/NORTE2020/Portugal 2020" for funding through project DESignBIOtechHealth (ref. Norte-01-0145-FEDER-000024). A fellowship from the Subprograma de Formación de Personal Investigador, MINECO, Spain, is acknowledged by E.M., and M.Q. is grateful to “Programa Nacional de Innovación para la competitividad y productividad” (Innóvate-Perú) for a PhD scholarship (grant 065-FINCYT-BDE-2014). ISGlobal and IBEC are members of the CERCA Programme, Generalitat de Catalunya.

**References**

[1] World Malaria Report. http://www.who.int/malaria/publications/world_malaria_report/en/. 2016. Geneva, Switzerland, World Health Organization.

[2] Guidelines for the treatment of malaria, 3rd edition. http://apps.who.int/iris/bitstream/10665/162441/1/9789241549127_eng.pdf. 2015. Geneva, Switzerland, World Health Organization.

[3] P.K. Sarkar, G. Ahluwalia, V.K. Vijayan, and A. Talwar, Critical care aspects of malaria, J. Intensive Care Med., 25 (2009) 93-103.

[4] A. Trampuz, M. Jereb, I. Muzlovic, and R.M. Prabhu, Clinical review: severe malaria, Crit. Care, 7 (2003) 315-323.

[5] E. Moles, K. Moll, J.H. Ch'ng, P. Parini, M. Wahlgren, and X. Fernàndez-Busquets, Development of drug-loaded immunoliposomes for the selective targeting and elimination of rosetting *Plasmodium falciparum*-infected red blood cells, J. Control. Release, 241 (2016) 57-67.

[6] J. Movellan, P. Urbán, E. Moles, J.M. de la Fuente, T. Sierra, J.L. Serrano, and X. Fernàndez-Busquets, Amphiphilic dendritic derivatives as nanocarriers for the targeted delivery of antimalarial drugs, Biomaterials, 35 (2014) 7940-7950.

[7] P. Urbán, J.J. Valle-Delgado, N. Mauro, J. Marques, A. Manfredi, M. Rottmann, E. Ranucci, P. Ferruti, and X. Fernàndez-Busquets, Use of poly(amidoamine) drug conjugates for the delivery of antimalarials to *Plasmodium*, J. Control. Release, 177 (2014) 84-95.

[8] P.A.M. Peeters, C. Oussoren, W.M.C. Eling, and D.J.A. Crommelin, Immunospecific targeting of immunoliposomes, F(ab')2 and IgG to red blood cells *in vivo*, Biochim. Biophys. Acta - Biomembranes, 943 (1988) 137-147.

[9] A.K. Agrawal, A. Singhal, and C.M. Gupta, Functional drug targeting to erythrocytes *in vivo* using antibody bearing liposomes as drug vehicles, Biochem. Biophys. Res. Commun., 148 (1987) 357-361.

[10] M. Owais, G.C. Varshney, A. Choudhury, S. Chandra, and C.M. Gupta, Chloroquine encapsulated in malaria-infected erythrocyte-specific antibody-bearing liposomes effectively controls chloroquine-resistant *Plasmodium berghei* infections in mice, Antimicrob. Agents Chemother., 39 (1995) 180-184.

[11] E. Moles, P. Urbán, M.B. Jiménez-Díaz, S. Viera-Morilla, I. Angulo-Barturen, M.A. Busquets, and X. Fernàndez-Busquets, Immunoliposome-mediated drug delivery to *Plasmodium*-infected and non-infected red blood cells as a dual therapeutic/prophylactic antimalarial strategy, J. Control. Release, 210 (2015) 217-229.

[12] M. Quiliano, A. Mendoza, K.Y. Fong, A. Pabón, N.E. Goldfarb, I. Fabing, A. Vettorazzi, A. López de Cerain, B.M. Dunn, G. Garavito, D.W. Wright, E. Deharo, S. Pérez-Silanes, I. Aldana, and S. Galiano, Exploring the scope of new arylamino alcohol derivatives: synthesis, antimalarial evaluation, toxicological studies, and target exploration, Int. J. Parasitol. Drugs Drug Resist., 6 (2016) 184-198.

[13] B.C. Pérez, C. Teixeira, I.S. Albuquerque, J. Gut, P.J. Rosenthal, J.R. Gomes, M. Prudêncio, and P. Gomes, N-cinnamoylated chloroquine analogues as dual-stage antimalarial leads, J. Med. Chem., 56 (2013) 556-567.

[14] M. Joshi, S. Pathak, S. Sharma, and V. Patravale, Design and *in vivo* pharmacodynamic evaluation of nanostructured lipid carriers for parenteral delivery of artemether: Nanoject, Int. J. Pharm., 364 (2008) 119-126.

[15] Wahajuddin, S.P. Singh, K.S. Raju, A. Nafis, S.K. Puri, and G.K. Jain, Intravenous pharmacokinetics, oral bioavailability, dose proportionality and *in situ* permeability of anti-malarial lumefantrine in rats, Malar. J., 10 (2011) 293.

[16] M.A. Travassos and M.K. Laufer, Resistance to antimalarial drugs: molecular, pharmacological and clinical considerations, Pediatr. Res., 65 (2009) 64R-70R.

[17] L. Cui, S. Mharakurwa, D. Ndiaye, P.K. Rathod, and P.J. Rosenthal, Antimalarial drug resistance: literature review and activities and findings of the ICEMR network, Am. J. Trop. Med. Hyg., 93 (2015) 57-68.

[18] C.H. Villa, A.C. Anselmo, S. Mitragotri, and V. Muzykantov, Red blood cells: supercarriers for drugs, biologicals, and nanoparticles and inspiration for advanced delivery systems, Adv. Drug Deliv. Rev., 106, Part A (2016) 88-103.

[19] A.C. Anselmo, V. Gupta, B.J. Zern, D. Pan, M. Zakrewsky, V. Muzykantov, and S. Mitragotri, Delivering nanoparticles to lungs while avoiding liver and spleen through adsorption on red blood cells, ACS Nano, 7 (2013) 11129-11137.

[20] E. Chambers and S. Mitragotri, Prolonged circulation of large polymeric nanoparticles by non-covalent adsorption on erythrocytes, J. Control. Release, 100 (2004) 111-119.

[21] C.A. Janeway, P. Travers, Jr., M. Walport, and M.J. Shlomchik, Immunobiology. The Immune System in Health and Disease, Garland Science, New York, 2001.

[22] R. van Wijk and W.W. van Solinge, The energy-less red blood cell is lost: erythrocyte enzyme abnormalities of glycolysis, Blood, 106 (2005) 4034.

[23] J.A. Virtanen, K.H. Cheng, and P. Somerharju, Phospholipid composition of the mammalian red cell membrane can be rationalized by a superlattice model, Proc. Natl. Acad. Sci. U. S. A., 95 (1998) 4964-4969.

[24] C.E. McLaren, G.M. Brittenham, and V. Hasselblad, Statistical and graphical evaluation of erythrocyte volume distributions, Am. J. Physiol. Heart Circ. Physiol., 252 (1987) H857.

[25] S.L. Schrier, What does the spleen see?, Blood, 120 (2012) 242.

[26] M.E. Reid, MNS blood group system: a review, Immunohematology, 25 (2009) 95-101.

[27] L. Dean, The MNS blood group, in: Belinda Beck (Ed.), Blood Groups and Red Cell Antigens (Internet), National Center for Biotechnology Information, Bethesda, MD, 2005, pp. 81-86.

[28] J.A. Chasis and N. Mohandas, Red blood cell glycophorins, Blood, 80 (1992) 1869.

[29] H.P. Fernandes, C.L. Cesar, and M.d.L. Barjas-Castro, Electrical properties of the red blood cell membrane and immunohematological investigation, Rev. Bras. Hematol. Hemoter., 33 (2011) 297-301.

[30] M. Salomao, X. Zhang, Y. Yang, S. Lee, J.H. Hartwig, J.A. Chasis, N. Mohandas, and X. An, Protein 4.1R-dependent multiprotein complex: new insights into the structural organization of the red blood cell membrane, Proc. Natl. Acad. Sci. U. S. A., 105 (2008) 8026-8031.

[31] N. Mohandas and P.G. Gallagher, Red cell membrane: past, present, and future, Blood, 112 (2008) 3939-3948.

[32] M. Petter, M. Haeggström, A. Khattab, V. Fernandez, M.Q. Klinkert, and M. Wahlgren, Variant proteins of the *Plasmodium falciparum* RIFIN family show distinct subcellular localization and developmental expression patterns, Mol. Biochem. Parasitol., 156 (2007) 51-61.

[33] K. Flick and Q. Chen, *var* genes, PfEMP1 and the human host, Mol. Biochem. Parasitol., 134 (2004) 3-9.

[34] S.M. Kraemer and J.D. Smith, A family affair: *var* genes, PfEMP1 binding, and malaria disease, Curr. Opin. Microbiol., 9 (2006) 374-380.

[35] K. Haldar, N. Mohandas, B.U. Samuel, T. Harrison, N.L. Hiller, T. Akompong, and P. Cheresh, Protein and lipid trafficking induced in erythrocytes infected by malaria parasites, Cell. Microbiol., 4 (2002) 383-395.

[36] L. Qiu, N. Jing, and Y. Jin, Preparation and *in vitro* evaluation of liposomal chloroquine diphosphate loaded by a transmembrane pH-gradient method, Int. J. Pharm., 361 (2008) 56-63.

[37] T.D. Madden, P.R. Harrigan, L.C.L. Tai, M.B. Bally, L.D. Mayer, T.E. Redelmeier, H.C. Loughrey, C.P.S. Tilcock, L.W. Reinish, and P.R. Cullis, The accumulation of drugs within large unilamellar vesicles exhibiting a proton gradient: a survey, Chem. Phys. Lipids, 53 (1990) 37-46.

[38] G. Stensrud, S. Sande, S. Kristensen, and G. Smistad, Formulation and characterisation of primaquine loaded liposomes prepared by a pH gradient using experimental design, Int. J. Pharm., 198 (2000) 213-228.

[39] M.B. Jiménez-Díaz, T. Mulet, V. Gómez, S. Viera, A. Alvarez, H. Garuti, Y. Vázquez, A. Fernández, J. Ibáñez, M. Jiménez, D. Gargallo-Viola, and I. Angulo-Barturen, Quantitative measurement of *Plasmodium*-infected erythrocytes in murine models of malaria by flow cytometry using bidimensional assessment of SYTO-16 fluorescence, Cytometry A, 75A (2009) 225-235.

[40] I. Angulo-Barturen, M.B. Jiménez-Díaz, T. Mulet, J. Rullas, E. Herreros, S. Ferrer, E. Jiménez, A. Mendoza, J. Regadera, P.J. Rosenthal, I. Bathurst, D.L. Pompliano, F. Gómez de las Heras, and D. Gargallo-Viola, A murine model of *falciparum*-malaria by *in vivo* selection of competent strains in non-myelodepleted mice engrafted with human erythrocytes, PLoS ONE, 3 (2008) e2252.

[41] Treatment of Malaria (Guidelines For Clinicians). Centers for Disease Control and Prevention. 2013.

[42] Y. Fu, Y. Ding, T.L. Zhou, Q.y. Ou, and W.y. Xu, Comparative histopathology of mice infected with the 17XL and 17XNL strains of *Plasmodium yoelii*, J. Parasitol., 98 (2012) 310-315.

[43] B. Pérez, C. Teixeira, J. Gut, P.J. Rosenthal, J.R.B. Gomes, and P. Gomes, Cinnamic acid/chloroquinoline conjugates as potent agents against chloroquine-resistant *Plasmodium falciparum*, ChemMedChem, 7 (2012) 1537-1540.

[44] ChemAxon, http://www.chemaxon.com. 2016.

[45] R.C. MacDonald, R.I. MacDonald, B.P. Menco, K. Takeshita, N.K. Subbarao, and L.R. Hu, Small-volume extrusion apparatus for preparation of large, unilamellar vesicles, Biochim. Biophys. Acta, 1061 (1991) 297-303.

[46] K. Moll, I. Ljungström, H. Perlmann, A. Scherf, and M. Wahlgren, Methods in Malaria Research, Malaria Research and Reference Reagent Resource Center (MR4), Manassas, VA, 2008.

[47] C. Lambros and J.P. Vanderberg, Synchronization of *Plasmodium falciparum* erythrocytic stages in culture, J. Parasitol., 65 (1979) 418-420.

[48] A. Radfar, D. Méndez, C. Moneriz, M. Linares, P. Marín-García, A. Puyet, A. Diez, and J.M. Bautista, Synchronous culture of *Plasmodium falciparum* at high parasitemia levels, Nat. Protoc., 4 (2009) 1899-1915.

[49] F. Omodeo-Salè, L. Cortelezzi, N. Basilico, M. Casagrande, A. Sparatore, and D. Taramelli, Novel antimalarial aminoquinolines: heme binding and effects on normal or *Plasmodium falciparum*-parasitized human erythrocytes, Antimicrob. Agents Chemother., 53 (2009) 4339-4344.

[50] A. Nair, B. Abrahamsson, D.M. Barends, D.W. Groot, S. Kopp, J.E. Polli, V.P. Shah, and J.B. Dressman, Biowaiver monographs for immediate-release solid oral dosage forms: primaquine phosphate, J. Pharm. Sci., 101 (2012) 936-945.

[51] T. Zhu, Z. Jiang, and Y. Ma, Lipid exchange between membranes: effects of membrane surface charge, composition, and curvature, Colloids Surf. B Biointerfaces, 97 (2012) 155-161.

[52] M. Koulnis, R. Pop, E. Porpiglia, J.R. Shearstone, D. Hidalgo, and M. Socolovsky, Identification and analysis of mouse erythroid progenitors using the CD71/TER119 flow-cytometric assay, J. Vis. Exp., (2011) 2809.

[53] A. Suzuki, S. Sekiya, M. Onishi, N. Oshima, H. Kiyonari, H. Nakauchi, and H. Taniguchi, Flow cytometric isolation and clonal identification of self-renewing bipotent hepatic progenitor cells in adult mouse liver, Hepatology, 48 (2008) 1964-1978.

[54] M.C. Woodle, M.S. Newman, and J.A. Cohen, Sterically stabilized liposomes: physical and biological properties, J. Drug Target., 2 (1994) 397-403.

[55] O.K. Nag, V.R. Yadav, A. Hedrick, and V. Awasthi, Post-modification of preformed liposomes with novel non-phospholipid poly(ethylene glycol)-conjugated hexadecylcarbamoylmethyl hexadecanoic acid for enhanced circulation persistence *in vivo*, Int. J. Pharm., 446 (2013) 119-129.

Supplementary data

# ImmunoPEGliposomes for the targeted delivery of novel lipophilic drugs to red blood cells in a falciparum malaria murine model

Ernest Moles[a,b,c,*], Silvia Galiano[d,e], Ana Gomes[f], Miguel Quiliano[d,e], Cátia Teixeira[f], Ignacio Aldana[d,e], Paula Gomes[f], Xavier Fernàndez-Busquets[a,b,c,*]

[a] Nanomalaria Group, Institute for Bioengineering of Catalonia (IBEC)
The Barcelona Institute of Science and Technology
Baldiri Reixac 10-12, ES-08028 Barcelona, Spain
[b] Barcelona Institute for Global Health (ISGlobal), Barcelona Center for International Health Research (CRESIB, Hospital Clínic-Universitat de Barcelona)
Rosselló 149-153, ES-08036 Barcelona, Spain
[c] Nanoscience and Nanotechnology Institute (IN2UB), University of Barcelona
Martí i Franquès 1, ES-08028 Barcelona, Spain
[d] Universidad de Navarra, Instituto de Salud Tropical (ISTUN), Campus Universitario
ES-31008 Pamplona, Spain
[e] Universidad de Navarra, Facultad de Farmacia y Nutrición
Departamento de Química Orgánica y Farmacéutica, Campus Universitario
ES-31008 Pamplona, Spain
[f] LAQV-REQUIMTE, Departamento de Química e Bioquímica
Faculdade de Ciências, Universidade do Porto
Rua do Campo Alegre 685, P-4169-007 Porto, Portugal

* Corresponding authors at: Nanomalaria Group, Barcelona Institute for Global Health (ISGlobal), Rosselló 149-153, ES-08036 Barcelona, Spain.
*E-mail addresses*: ernest.moles@isglobal.org; xfernandez_busquets@ub.edu

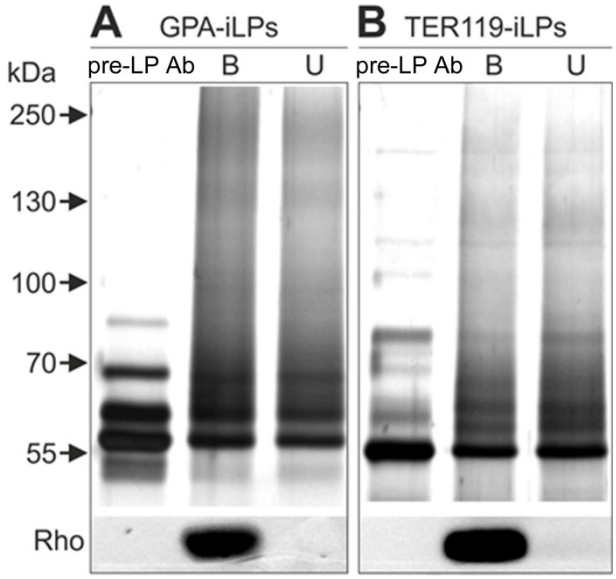


**Fig. S1.** SDS-PAGE qualitative analysis of the optimized coupling to LPs of RBC-specific antibodies. For each Ab are shown liposome-bound (B) and unbound (U) fractions as well as the original (pre-LP) Ab fraction used (all lanes contain 2 µg protein). (A) GPA-iLP conjugation using 10× SATA:Ab and 50 µg Ab/µmol lipid. (B) TER119-iLP conjugation using 5× SATA:Ab and 100 µg Ab/µmol lipid. Respective anti-GPA and TER119 Ab conjugation efficiencies of 67.3 ± 4.6% and 39.6 ± 3.2% were quantitatively determined as described in Materials and methods. The fluorescence emission of the rhodamine-conjugated lipid (DOPE-Rho) is included as control for LP-containing fractions.

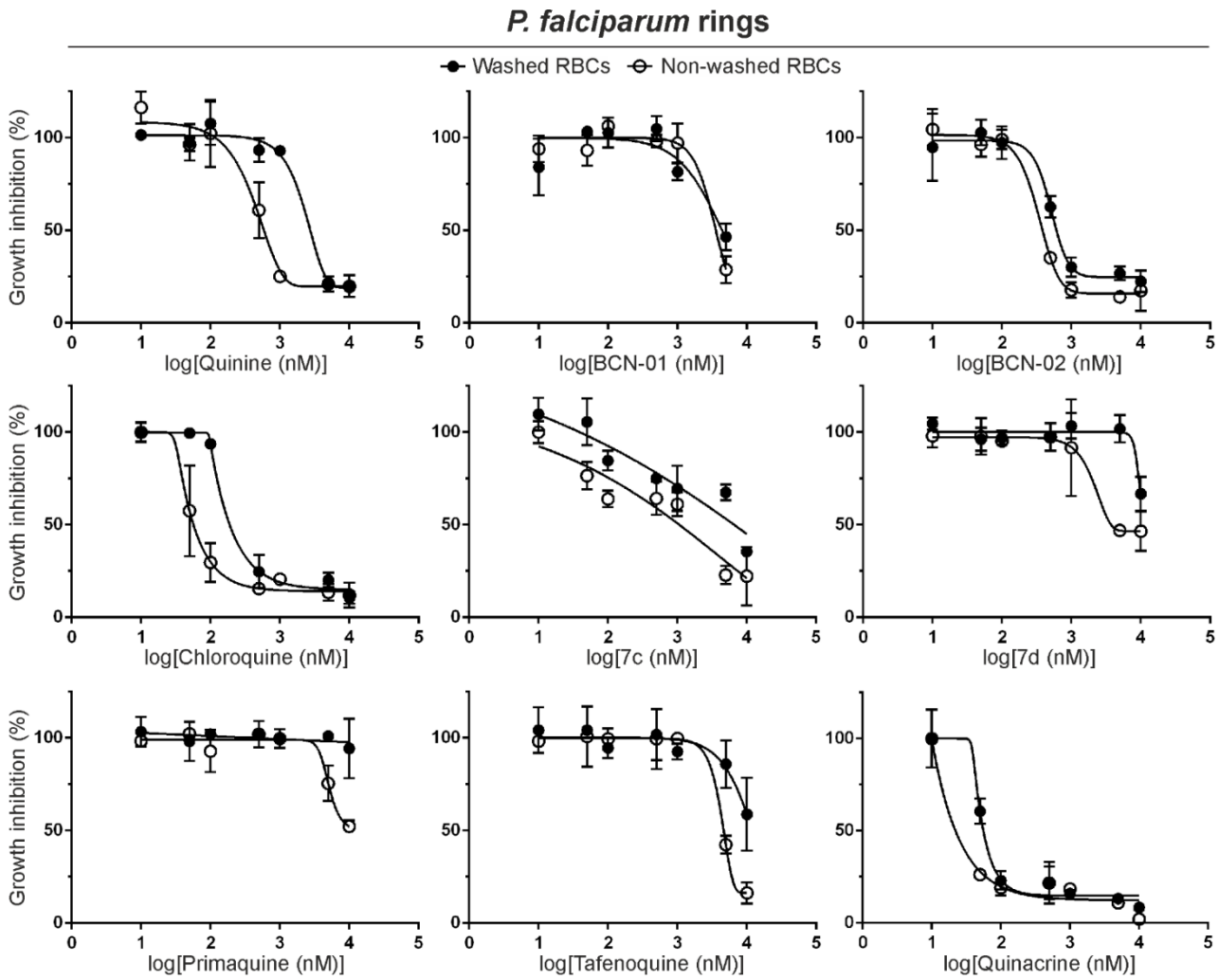


**Fig. S2.** Analysis of the prophylactic performance of antimalarials pre-loaded in RBCs prior to infection with pRBCs containing *P. falciparum* parasites at the ring (early) stage. The results are expressed as parasite growth inhibition rates relative to an untreated culture (100% growth). Washed and non-washed conditions refer, respectively, to samples where drug which did not enter RBCs was either removed or left in the cultures until the end of the assay. Drug concentrations refer to those initially added at the start of the assays.

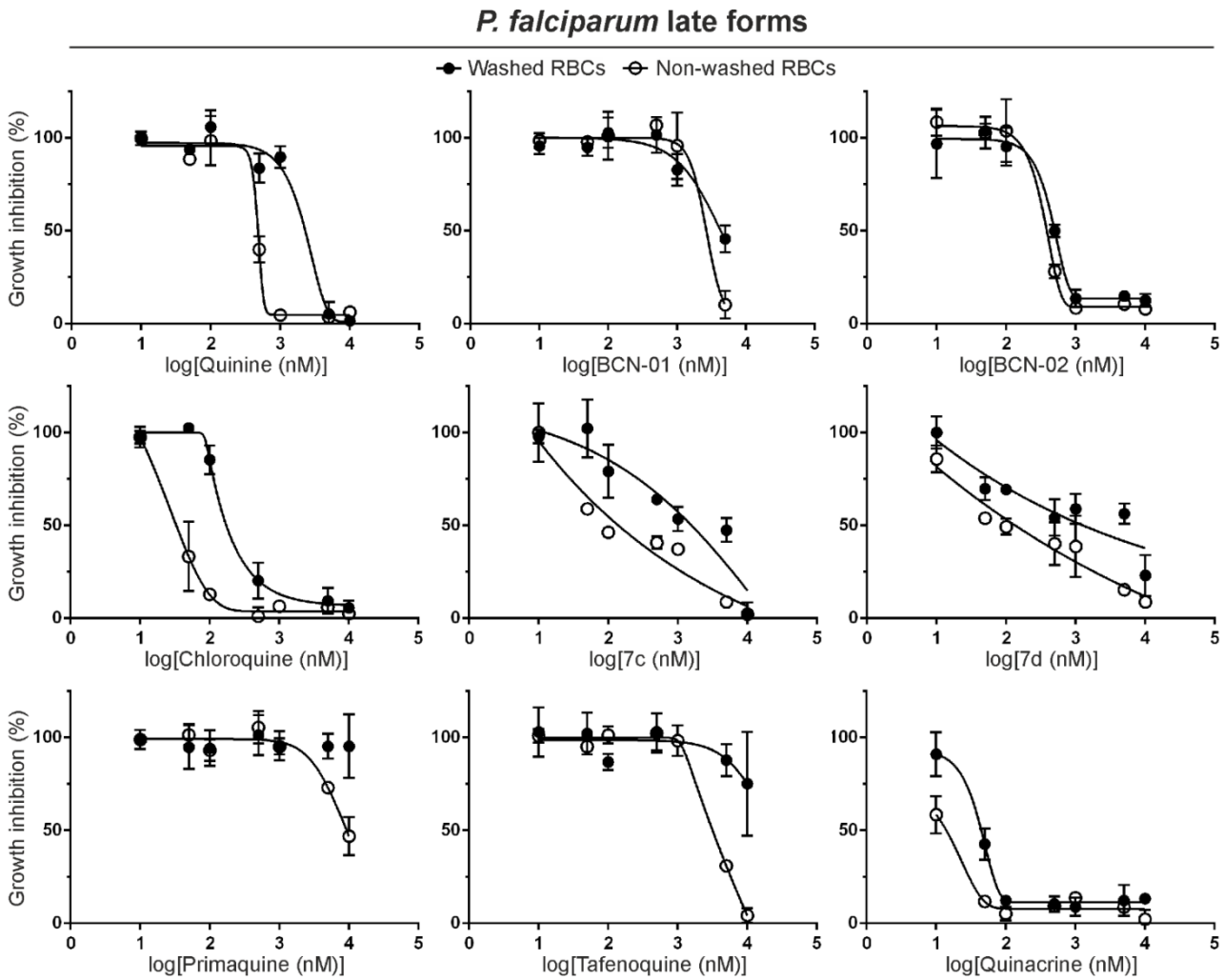


**Fig. S3.** Analysis of the prophylactic performance of antimalarials pre-loaded in RBCs prior to infection with pRBCs containing *P. falciparum* parasites at late stages. The results are expressed as parasite growth inhibition rates relative to an untreated culture (100% growth). Washed and non-washed conditions refer, respectively, to samples where drug which did not enter RBCs was either removed or left in the cultures until the end of the assay. Drug concentrations refer to those initially added at the start of the assays.

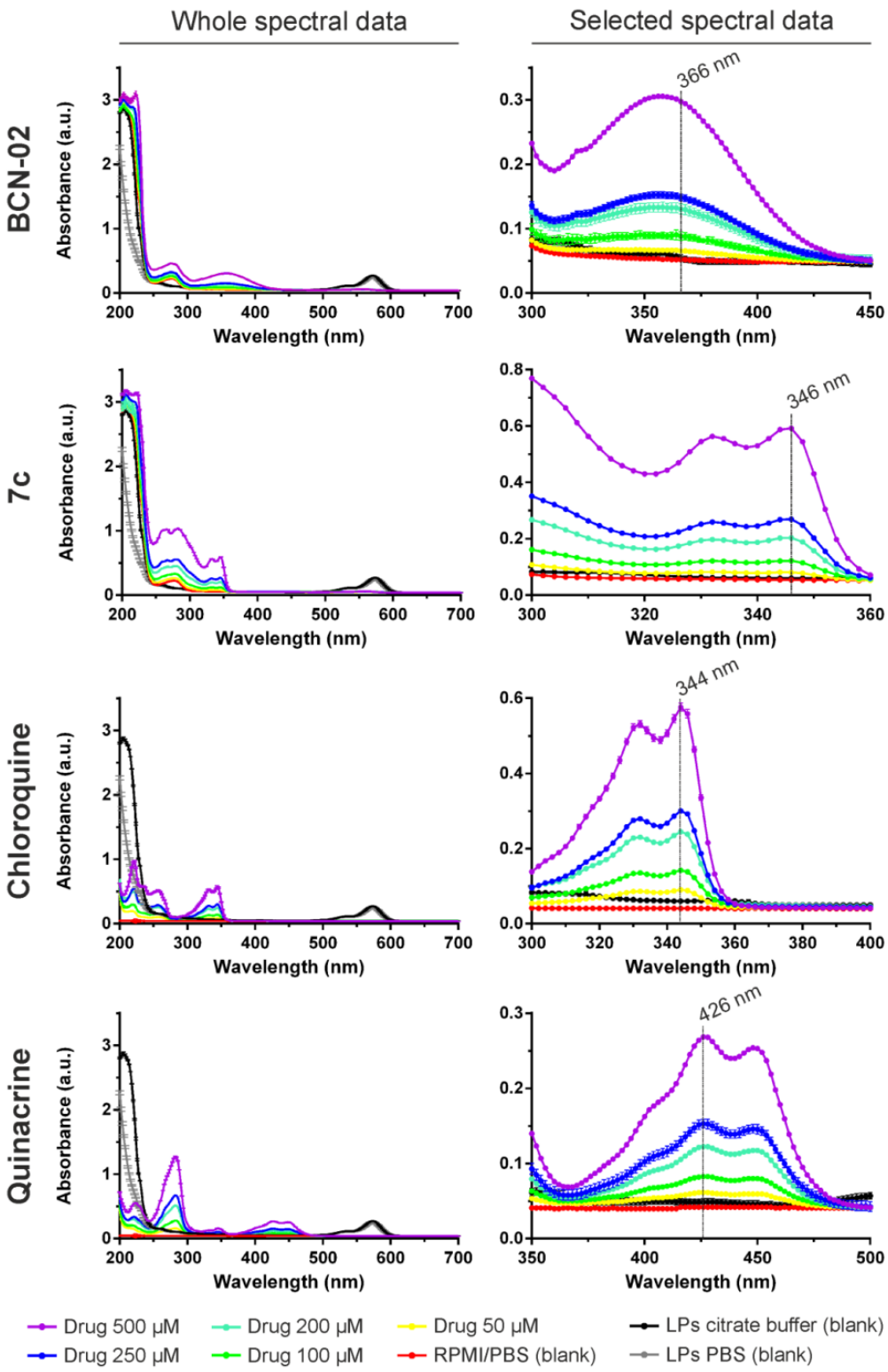


**Fig. S4.** UV/visible absorption spectra for the quantification of actively encapsulated drugs into LPs. Whole (200- to 700-nanometer wavelength range) as well as drug-selected spectra (arbitrary units, a.u.) were retrieved at the end of the encapsulation process for all LP[drug] samples after SDS-digestion and sonication as detailed in Materials and methods. Spectra from RPMI-dissolved free drug standards (50-500 µM concentration range) were analyzed for calibration curve determination. Specific wavelengths used for calibration of each drug are indicated.

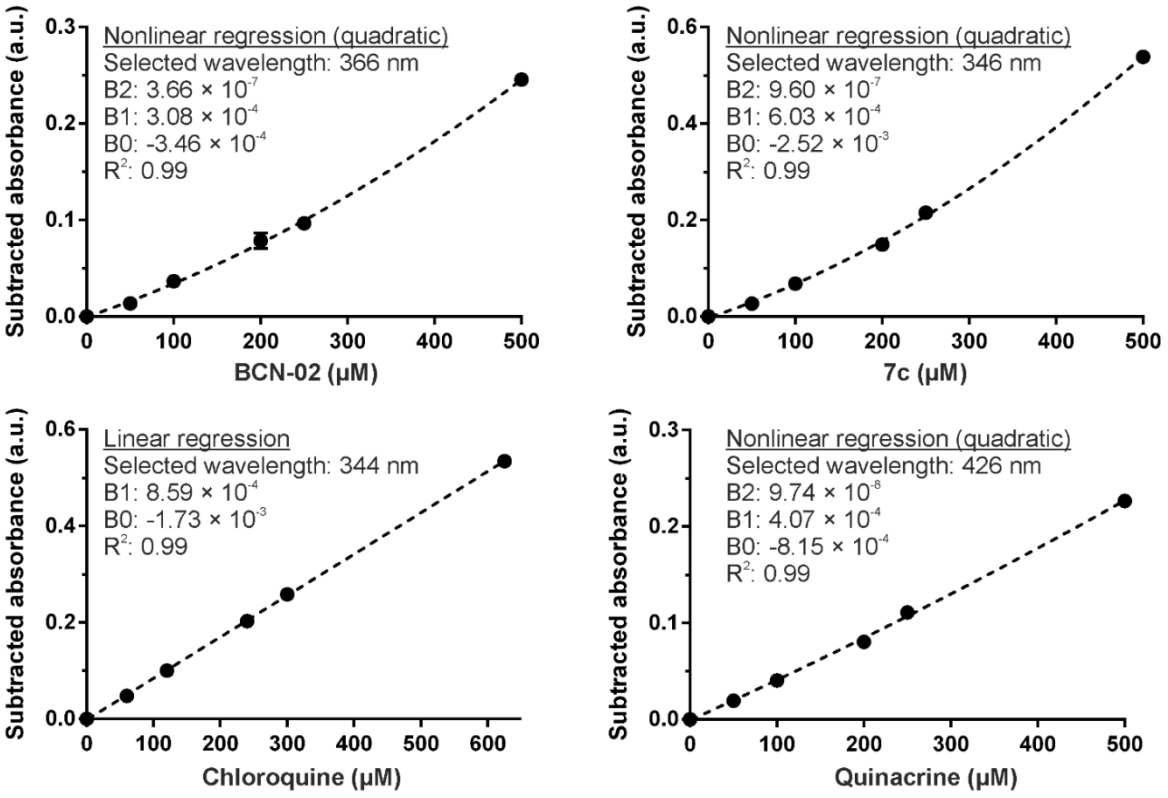


**Fig. S5.** Linear and quadratic calibration curves derived from the spectral data in Fig. S4, and used for drug quantification after active encapsulation in LPs. RPMI buffer absorption at the respective drug-specific wavelengths was taken as absorbance subtraction blank.

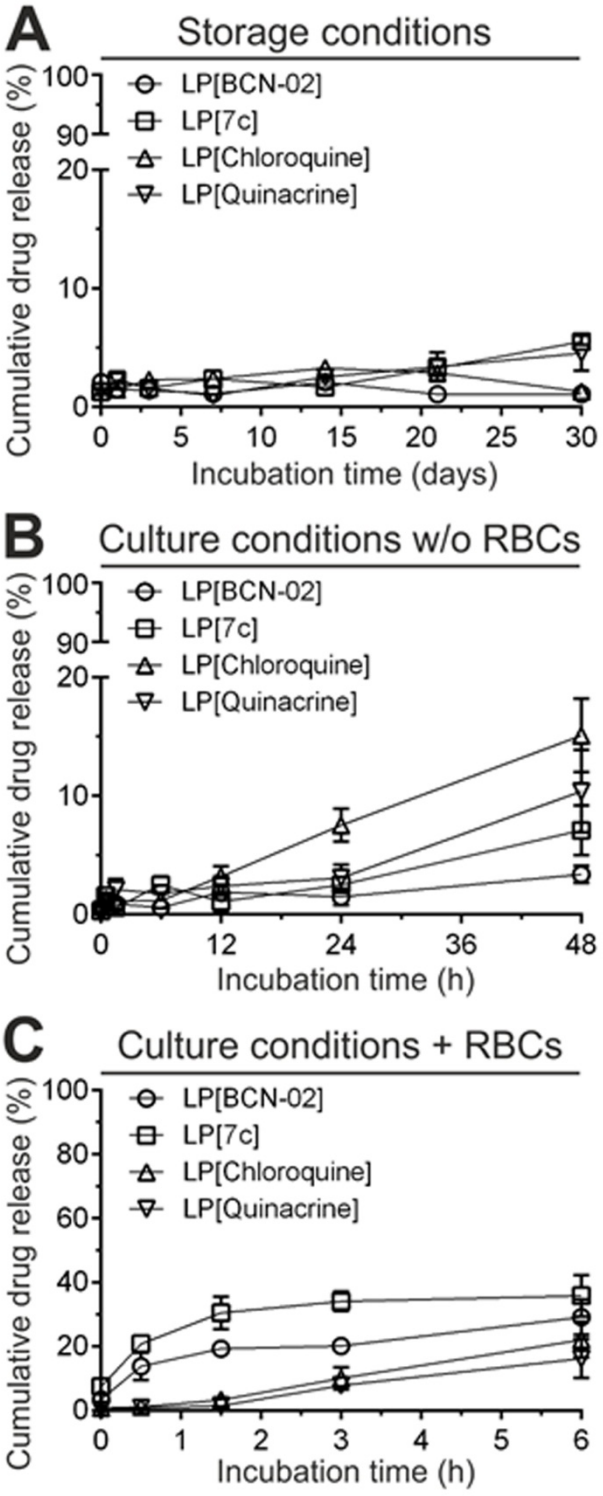


**Fig. S6.** Analysis of the stability of liposomal preparations actively encapsulating antimalarial drugs. Percentual cumulative drug release under (A) storage conditions (PBS, 4 °C, 10 mM lipid) and (B,C) *in vitro* culture conditions (RPMI-A, 37 °C, 2 mM lipid) in (B) the absence or (C) presence of red blood cells at 10% hematocrit (50 µM encapsulated drug along with 2 mM lipid during incubation, corresponding to the highest [drug]/hematocrit ratio used in *P. falciparum* growth inhibition assays).

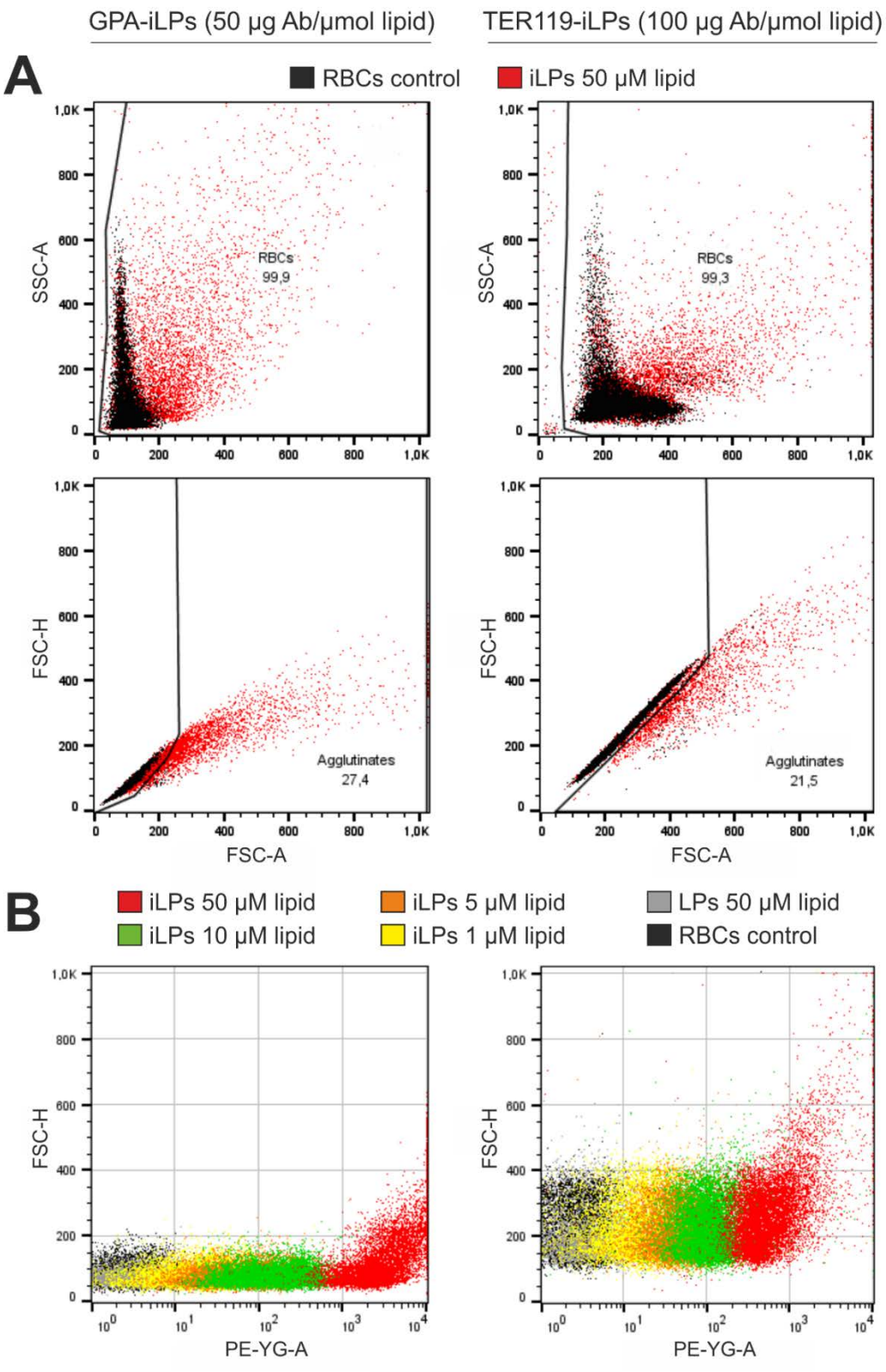


**Fig. S7.** Flow cytometry results from optimization experiments for GPA- and TER119-iLP targeting performance towards erythrocyte suspensions *in vitro*. (A) Selection of the RBC population and determination of RBC agglutinates (% of total cells, FSC-H vs. FSC-A confronted channels) as described in Materials and methods. (B) Retrieved plots for rhodamine-labeled iLP targeting analysis (rhodamine signal detected in PE-YG channel). RBCs alone and non-targeted LPs are included as negative controls.

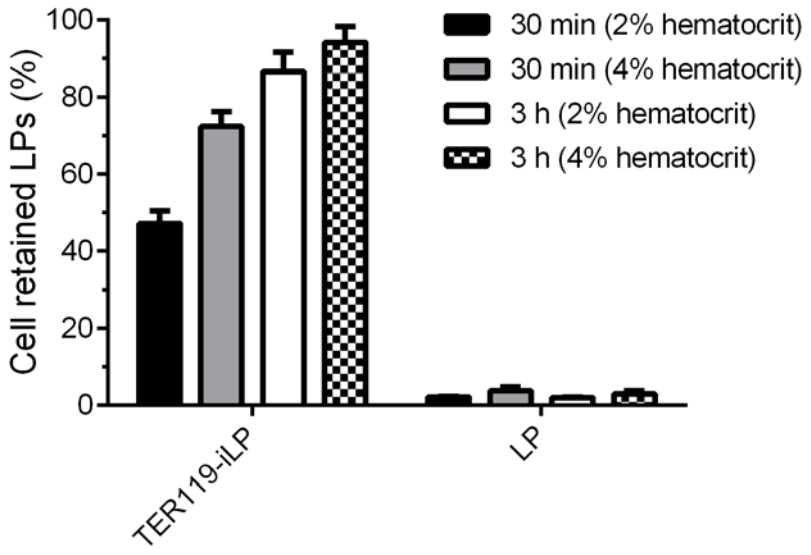


**Fig. S8.** Improvement in mouse RBC retention *in vitro* efficacy of 5× SATA:Ab TER119-iLPs using larger hematocrits and longer incubation times. Non-targeted LPs are included as negative control. Results were obtained by rhodamine fluorescence quantification and are expressed as % of cell-bound LPs relative to the total number of LPs (20 μM total lipid concentration) ± standard deviation for at least three independent measurements.

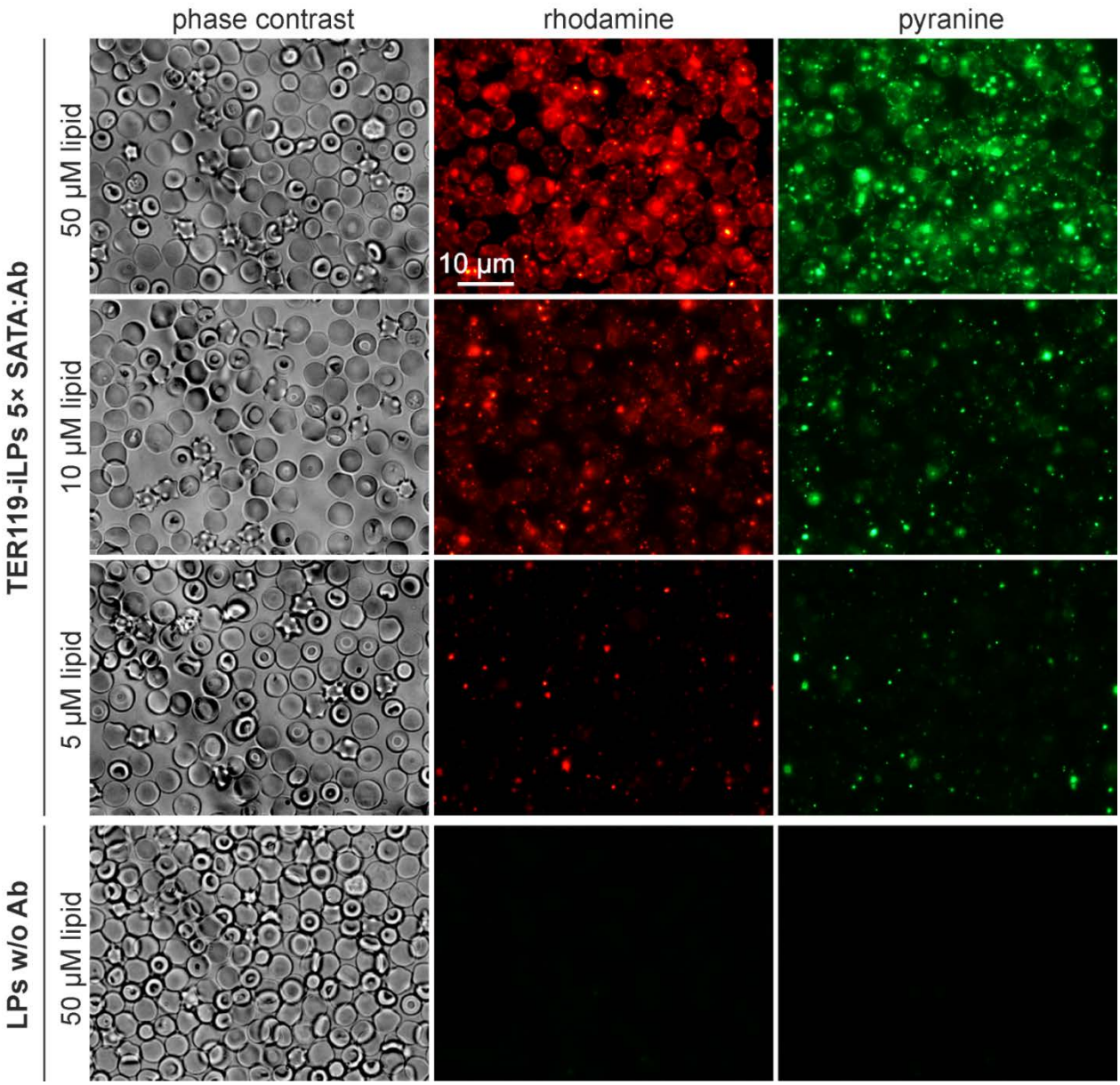


**Fig. S9.** Fluorescence microscopy targeting results for the improved 5× SATA:Ab TER119-iLP model assayed *in vitro* in mouse RBC suspensions. LP surface/contents are shown by rhodamine/pyranine fluorescence emission at different total lipid concentrations after 30 min incubation. Non-targeted LPs (LPs w/o Ab) are included as negative targeting control sample.

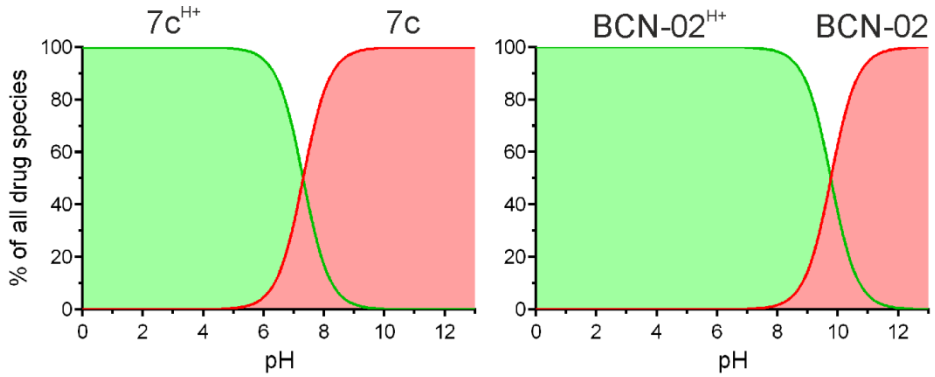


**Fig. S10.** Ionization molecular species found in solution as a function of pH for 7c and BCN-02. Abundances were calculated using the drug pKa values from Table 1.

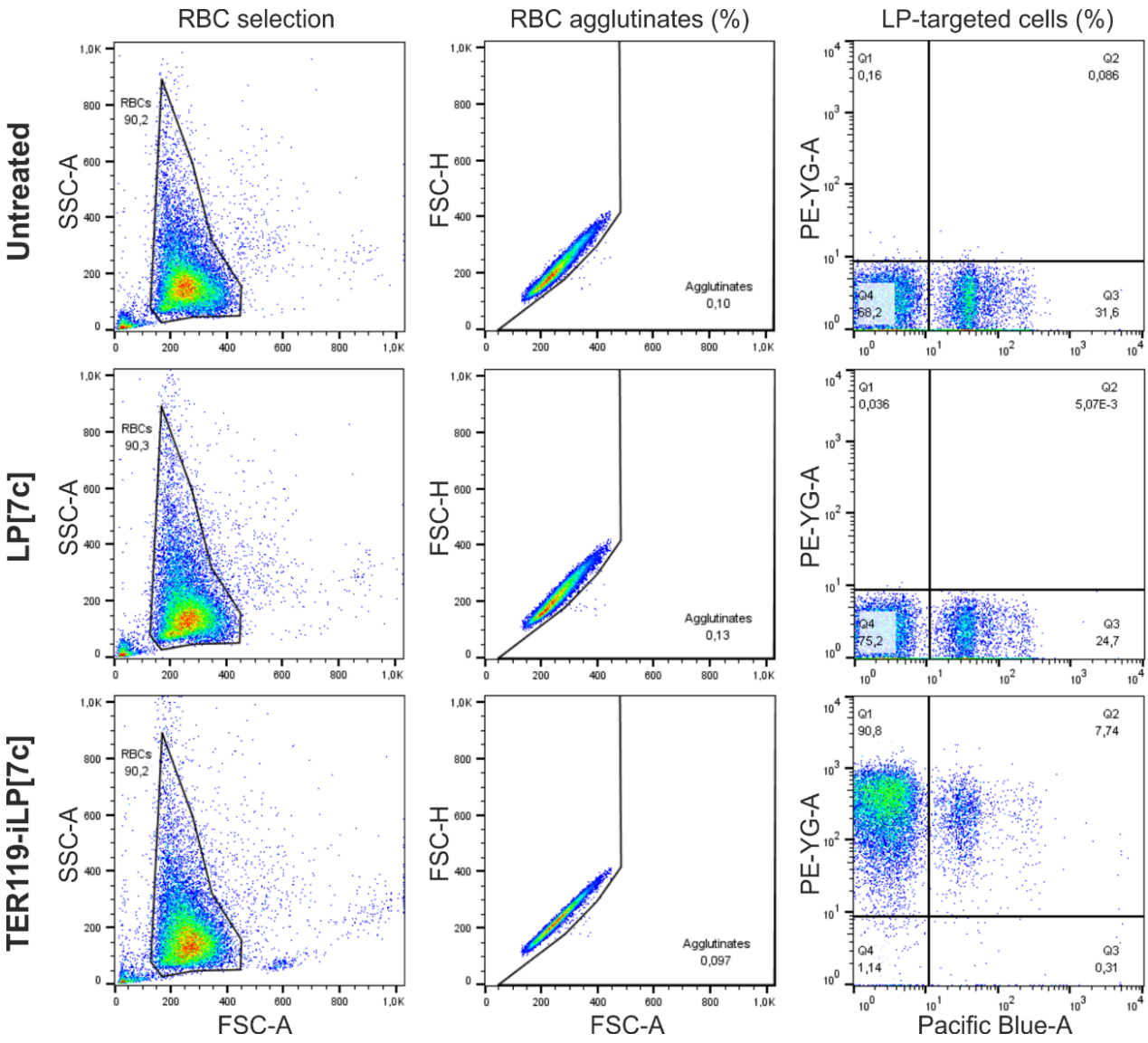


**Fig. S11.** *In vivo* study of the antimalarial performance of TER119-iLP[7c] (5× SATA:Ab) in *P. yoelii* 17XL-infected immunocompetent mice. The summary of flow cytometry data shows RBC agglutinating and targeting results obtained for untreated, LP[7c]-treated, and TER119-iLP[7c]-treated mouse blood samples on day 3 post-infection. Pacific Blue-A and PE-YG channels are included for the analysis of pRBC nuclei (Hoechst 33342) and LP-associated (rhodamine) fluorescence signals, respectively. RBC agglutinates (%) from total cells in suspension were determined by FSC-H vs. FSC-A confronted channels as detailed in Materials and methods.

**Table S1.** Determination of statistical differences from the *P. falciparum* growth inhibition assays in Figs. S2 and S3. Parasite growth is expressed as $\log_{10}$(IC50, nM) ± standard deviation from at least three experimental replicates. Impaired t-test *p* values are included in the table comparing $\log_{10}$(IC50, nM) results from washed vs. non-washed RBC culture conditions. NA: not analyzable.

| | $\log_{10}$(IC50, nM) ± SD | | |
|---|---|---|---|
| | Washed RBCs | Non-washed RBCs | *p* value |
| | Rings | | |
| Quinine | 3.36 ± 0.15 | 2.64 ± 0.13 | $3.3\times10^{-3}$ |
| BCN-01 | 3.64 ± 0.13 | 3.55 ± 0.09 | 0.39 |
| BCN-02 | 2.71 ± 0.06 | 2.52 ± 0.13 | 0.09 |
| Chloroquine | 2.21 ± 0.09 | 1.70 ± 0.07 | $1.4\times10^{-3}$ |
| 7c | 3.70 ± 2.45 | 3.02 ± 2.00 | 0.73 |
| 7d | NA | 3.33 ± 0.79 | NA |
| Primaquine | NA | ~3.71 | NA |
| Tafenoquine | 3.96 ± 1.91 | 3.63 ± 2.48 | 0.87 |
| Quinacrine | 1.71 ± 1.07 | 1.28 ± 0.43 | 0.55 |
| | Late forms | | |
| Quinine | 3.37 ± 0.18 | 2.68 ± 0.14 | 0.01 |
| BCN-01 | 3.63 ± 0.09 | 3.42 ± 0.15 | 0.10 |
| BCN-02 | 2.66 ± 0.23 | 2.54 ± 0.11 | 0.48 |
| Chloroquine | 2.21 ± 0.50 | 1.25 ± 0.11 | 0.03 |
| 7c | 3.50 ± 2.38 | 1.37 ± 0.93 | 0.22 |
| 7d | 1.69 ± 0.42 | 2.04 ± 0.39 | 0.35 |
| Primaquine | NA | 3.93 ± 1.29 | NA |
| Tafenoquine | NA | 4.95 ± 3.32 | NA |
| Quinacrine | 1.63 ± 0.27 | 1.31 ± 0.33 | 0.26 |

**Table S2.** Analysis of drug interaction with LPs during the citrate-buffered, pH gradient-based active encapsulation process for BCN-01, BCN-02, 7c and 7d. LP surface charge and size results were obtained from 500 µM/10 mM drug/lipid mixtures, expressed as mean ζ potential (mV) and diameter (nm), respectively, with the corresponding standard deviation from three individual measurements and determined before and after the buffer exchange (BE) step required for the removal of non-encapsulated contents. Because no differences in particle size and polydispersity index (PDI) were observed between control and drug-containing LPs, mean particle size and PDI are provided for each group of samples. *p* values are included in the table comparing results from LP control vs. LP[drug] samples.

| | | *p* values | | | |
|---|---|---|---|---|---|
| | Mean ζ-potential (mV) ± SD | LP[BCN-01] | LP[BCN-02] | LP[7c] | LP[7d] |
| | LPs in citrate (mean particle size: 203.9 ± 2.1 nm; PDI: 0.25 ± 0.02) | | | | |
| LP | -2.61 ± 0.20 | $2.39 \times 10^{-6}$ | $9.92 \times 10^{-10}$ | $2.98 \times 10^{-10}$ | $7.25 \times 10^{-5}$ |
| LP[BCN-01] | 6.61 ± 0.24 | - | $8.31 \times 10^{-4}$ | $5.23 \times 10^{-4}$ | $3.86 \times 10^{-6}$ |
| LP[BCN-02] | 8.43 ± 0.15 | - | - | $4.70 \times 10^{-6}$ | $1.44 \times 10^{-6}$ |
| LP[7c] | 4.05 ± 0.12 | - | - | - | $7.07 \times 10^{-5}$ |
| LP[7d] | -0.12 ± 0.21 | - | - | - | - |
| | LPs after BE (mean particle size: 177.4 ± 1.7 nm; PDI: 0.12 ± 0.03) | | | | |
| LP | -17.55 ± 1.18 | 0.56 | 0.81 | 0.64 | 0.78 |
| LP[BCN-01] | -16.63 ± 2.20 | - | 0.64 | 0.69 | 0.65 |
| LP[BCN-02] | -17.37 ± 0.96 | - | - | 0.86 | 0.97 |
| LP[7c] | -17.23 ± 0.76 | - | - | - | 0.89 |
| LP[7d] | -17.33 ± 0.96 | - | - | - | - |

**Table S3.** Determination of statistical differences in *P. falciparum* growth inhibition assays for the analysis of GPA-iLP[drug] antimalarial activity *in vitro*. Parasite growth in cultures of the CQ-sensitive/resistant 3D7/W2mef strains at either ring (early) or late *P. falciparum* blood stages is expressed as $\log_{10}$(IC50, nM) ± standard deviation from at least three experimental replicates. Impaired t-test *p* values are included in the table comparing $\log_{10}$(IC50, nM) results from free drug vs. iLP[drug] culture conditions.

| | $\log_{10}$[IC50 (nM)] ± SD | | |
|---|---|---|---|
| | Free drug | iLP[drug] | *p* value |
| | Rings (3D7) | | |
| BCN-02 | $3.01 \pm 4.32 \times 10^{-3}$ | $2.25 \pm 1.92 \times 10^{-3}$ | $<1 \times 10^{-4}$ |
| 7c | 3.08 ± 0.07 | 1.84 ± 0.03 | $<1 \times 10^{-4}$ |
| Chloroquine | 2.24 ± 0.09 | 1.75 ± 0.02 | $9 \times 10^{-4}$ |
| Quinacrine | 2.04 ± 0.04 | 1.65 ± 0.03 | $<1 \times 10^{-4}$ |
| | Late forms (3D7) | | |
| BCN-02 | 3.03 ± 0.03 | 2.29 ± 0.02 | $<1 \times 10^{-4}$ |
| 7c | 3.07 ± 0.04 | $2.00 \pm 3.06 \times 10^{-3}$ | $<1 \times 10^{-4}$ |
| Chloroquine | 2.24 ± 0.09 | 1.71 ± 0.05 | $1 \times 10^{-3}$ |
| Quinacrine | 2.01 ± 0.02 | 1.65 ± 0.02 | $<1 \times 10^{-4}$ |
| | Late forms (W2mef) | | |
| 7c | 3.11 ± 0.05 | 1.69 ± 0.03 | $<1 \times 10^{-4}$ |
| Chloroquine | 3.38 ± 0.19 | $2.81 \pm 4.12 \times 10^{-3}$ | 0.01 |

**Table S4.** MTD assay of intraperitoneally administered BCN-02 formulated in a 10% v/v chloroform/RPMI-A emulsion and following a 4-day dosage regime. Toxicity results are expressed from individually treated mice as animal weight (g) along with the corresponding weight loss (%) on the day of study relative to the start of the assay (Day 0). The four days when drug was injected are indicated in bold. (*) Dead animal, weighted animal corpse. (**) Amount of chloroform corresponding to the 50 mg/kg dose administered of BCN-02.

| | Weight of mice (g) | | | | | | | | | | | | | | | | |
|---|---|---|---|---|---|---|---|---|---|---|---|---|---|---|---|---|---|
| | **Day 0** | **Day 1** | % | **Day 2** | % | **Day 3** | % | Day 4 | % | Day 5 | % | Day 6 | % | Day 7 | % | Day 8 | % |
| Emulsified BCN-02 | | | | | | | | | | | | | | | | | |
| 50 mg/kg | 18.50 | 17.95* | -2.97 | - | - | - | - | - | - | - | - | - | - | - | - | - | - |
| 20 mg/kg | 20.13 | 19.33 | -3.97 | 18.93* | -5.98 | - | - | - | - | - | - | - | - | - | - | - | - |
| 10 mg/kg | 18.60 | 17.87 | -3.94 | 18.00 | -3.23 | 18.03 | -3.05 | 18.03 | -3.05 | 18.32 | -1.51 | 18.23 | -1.99 | 18.25 | -1.88 | 18.12 | -2.58 |
| 5 mg/kg | 19.40 | 18.97 | -2.23 | 19.40 | 0.00 | 19.40 | 0.00 | 19.10 | -1.55 | 19.23 | -0.88 | 19.12 | -1.44 | 19.24 | -0.82 | 19.13 | -1.39 |
| 1 mg/kg | 18.43 | 18.03 | -2.17 | 18.50 | 0.36 | 18.90 | 2.53 | 18.57 | 0.72 | 18.52 | 0.47 | 18.68 | 1.34 | 18.58 | 0.80 | 18.61 | 0.96 |
| 0 mg/kg | 19.03 | 18.67 | -1.93 | 18.97 | -0.35 | 19.07 | 0.18 | 18.57 | -2.45 | 18.82 | -1.12 | 19.02 | -0.07 | 18.75 | -1.49 | 18.69 | -1.80 |
| Chloroform/RPMI-A 10% v/v | | | | | | | | | | | | | | | | | |
| 10% v/v ** | 19.72 | 19.78 | 0.30 | 19.82 | 0.51 | 19.74 | 0.10 | 19.45 | -1.37 | 19.57 | -0.76 | 19.68 | -0.20 | 19.35 | -1.88 | 19.71 | -0.05 |

**Table S5.** MTD assay of intravenously administered 7c and BCN-02 formulated in 10% v/v chloroform/RPMI-A emulsion. Individual mice were treated at day 0 with the indicated single doses. Toxicity is determined by animal weight (g) along with the corresponding weight loss (%) on the day of study relative to day 0. ($^{\dagger}$) Dead animal within the day of administration. (*) Significant loss in animal weight (>10%). (**) Dead animal, weighted animal corpse.

| | Weight of mice (g) | | | | | | |
|---|---|---|---|---|---|---|---|
| | **Day 0** | Day 1 | % | Day 2 | % | Day 3 | % |
| Emulsified 7c | | | | | | | |
| 10 mg/kg | 20.62$^{\dagger}$ | - | - | - | - | - | - |
| 5 mg/kg | 20.23$^{\dagger}$ | - | - | - | - | - | - |
| 2.5 mg/kg | 21.41 | 19.22* | -10.23 | 18.78** | -12.28 | - | - |
| 1 mg/kg | 20.82 | 19.25 | -7.54 | 19.19 | -7.83 | 18.56** | -10.85 |
| 0 mg/kg | 21.04 | 21.08 | 0.19 | 20.98 | -0.29 | 21.12 | 0.38 |
| Emulsified BCN-02 | | | | | | | |
| 10 mg/kg | 22.49$^{\dagger}$ | - | - | - | - | - | - |
| 5 mg/kg | 19.78$^{\dagger}$ | - | - | - | - | - | - |
| 2.5 mg/kg | 20.55 | 18.02** | -12.31 | - | - | - | - |
| 1 mg/kg | 21.25 | 19.56 | -7.95 | 19.02* | -10.49 | 18.89** | -11.11 |
| 0 mg/kg | 20.91 | 21.15 | 1.15 | 21.24 | 1.58 | 21.11 | 0.96 |
| Chloroform/RPMI-A | | | | | | | |
| 10% v/v | 21.44 | 19.95 | -6.95 | 19.85 | -7.42 | 19.53 | -8.91 |

**Table S6.** MTD assay of passively encapsulated, non-targeted LP[7c] and LP[BCN-02] formulations, intravenously administered following a 4-day dosage regime. Toxicity results are expressed from individually treated mice as animal weight (g) along with the corresponding weight loss (%) on the day of study relative to the start of the assay (Day 0). The four days at which LP[drug] samples were injected are indicated in bold. (*) Significant loss in animal weight (>10%). (**) Dead animal, weighted animal corpse.

| | Weight of mice (g) | | | | | | | | | | | | | | | |
|---|---|---|---|---|---|---|---|---|---|---|---|---|---|---|---|---|
| | **Day 0** | **Day 1** | % | **Day 2** | % | **Day 3** | % | Day 4 | % | Day 5 | % | Day 6 | % | Day 7 | % | Day 8 | % |
| LP[7c] | | | | | | | | | | | | | | | | | |
| 20 mg/kg | 19.32 | 19.18 | -0.72 | 19.60 | 1.45 | 19.31 | -0.05 | 19.43 | 0.57 | 18.57 | -3.88 | 19.02 | -1.55 | 17.23 | -10.82* | 16.93** | -12.37* |
| 10 mg/kg | 22.25 | 22.13 | -0.54 | 21.80 | -2.02 | 22.30 | 0.22 | 21.76 | -2.20 | 21.59 | -2.97 | 22.19 | -0.27 | 21.62 | -2.83 | 21.7 | -2.47 |
| 5 mg/kg | 24.79 | 25.28 | 1.98 | 24.30 | -1.98 | 24.55 | -0.97 | 24.53 | -1.05 | 24.48 | -1.25 | 24.56 | -0.93 | 24.35 | -1.77 | 24.25 | -2.18 |
| 1 mg/kg | 23.42 | 23.80 | 1.62 | 23.05 | -1.58 | 23.04 | -1.62 | 23.37 | -0.21 | 23.28 | -0.60 | 23.52 | 0.43 | 23.05 | -1.58 | 22.74 | -2.90 |
| 0 mg/kg | 21.35 | 21.05 | -1.41 | 21.30 | -0.23 | 21.51 | 0.75 | 21.52 | 0.80 | 21.43 | 0.37 | 21.29 | -0.28 | 21.36 | 0.05 | 20.76 | -2.76 |
| LP[BCN-02] | | | | | | | | | | | | | | | | | |
| 20 mg/kg | 21.05 | 20.95 | -0.48 | 21.03 | -0.10 | 21.12 | 0.33 | 21.07 | 0.10 | 20.95 | -0.48 | 21.09 | 0.19 | 20.64 | -1.95 | 20.54 | -2.42 |
| 10 mg/kg | 21.26 | 21.30 | 0.19 | 21.20 | -0.28 | 21.22 | -0.19 | 21.13 | -0.61 | 21.12 | -0.66 | 21.24 | -0.09 | 20.78 | -2.26 | 20.82 | -2.07 |
| 5 mg/kg | 21.12 | 21.07 | -0.24 | 21.15 | 0.14 | 20.58 | -2.56 | 20.19 | -4.40 | 20.53 | -2.79 | 21.08 | -0.19 | 20.49 | -2.98 | 20.62 | -2.37 |
| 1 mg/kg | 21.01 | 20.85 | -0.76 | 21.60 | 2.81 | 20.88 | -0.62 | 20.72 | -1.38 | 20.78 | -1.09 | 21.12 | 0.52 | 21.28 | 1.29 | 21.05 | 0.19 |
| 0 mg/kg | 22.49 | 22.55 | 0.27 | 22.50 | 0.04 | 22.30 | -0.84 | 22.80 | 1.38 | 22.42 | -0.31 | 22.24 | -1.11 | 21.96 | -2.36 | 22.03 | -2.05 |

**Table S7.** *In vivo* toxicity results obtained for the intravenously administered LP[7c] and TER119-iLP[7c] actively-encapsulated antimalarial formulations from Fig. 6. Toxicity results are expressed as mean mouse weight (g) from at least three independent animal replicates along with the corresponding weight loss (%) on the day of study relative to the start of the assay (Day 0). The days at which LP[drug] samples were injected have been labeled in bold.

| | Mice (n = 3) | **Day 0** | **Day 1** | % | **Day 2** | % | Day 3 | % |
|---|---|---|---|---|---|---|---|---|
| iLP[7c] | M1 | 17.97 | 16.98 | -5.51 | 16.91 | -5.89 | 17.21 | -4.24 |
| | M2 | 15.62 | 15.30 | -6.83 | 14.50 | -7.18 | 14.75 | -5.55 |
| | M3 | 17.11 | 15.90 | -7.07 | 15.87 | -7.22 | 16.16 | -5.56 |
| | Mean | 16.90 | 16.06 | -6.47 | 15.76 | -6.76 | 16.04 | -5.12 |
| LP[7c] | M1 | 17.97 | 18.21 | 1.34 | 17.90 | -0.39 | 17.90 | -0.39 |
| | M2 | 15.07 | 15.51 | 2.92 | 15.30 | 1.53 | 15.30 | 1.53 |
| | M3 | 17.81 | 18.14 | 1.85 | 17.50 | -1.74 | 18.10 | 1.63 |
| | Mean | 16.95 | 17.29 | 2.04 | 16.90 | -0.20 | 17.10 | 0.92 |
| Untreated | M1 | 18.03 | 17.66 | -2.05 | 17.20 | -4.60 | 17.80 | -1.28 |
| | M2 | 16.70 | 17.40 | 4.19 | 17.10 | 2.40 | 17.40 | 4.19 |
| | M3 | 15.84 | 16.78 | 5.93 | 16.80 | 6.06 | 16.50 | 4.17 |
| | Mean | 16.86 | 17.28 | 2.69 | 17.03 | 1.28 | 17.23 | 2.36 |